

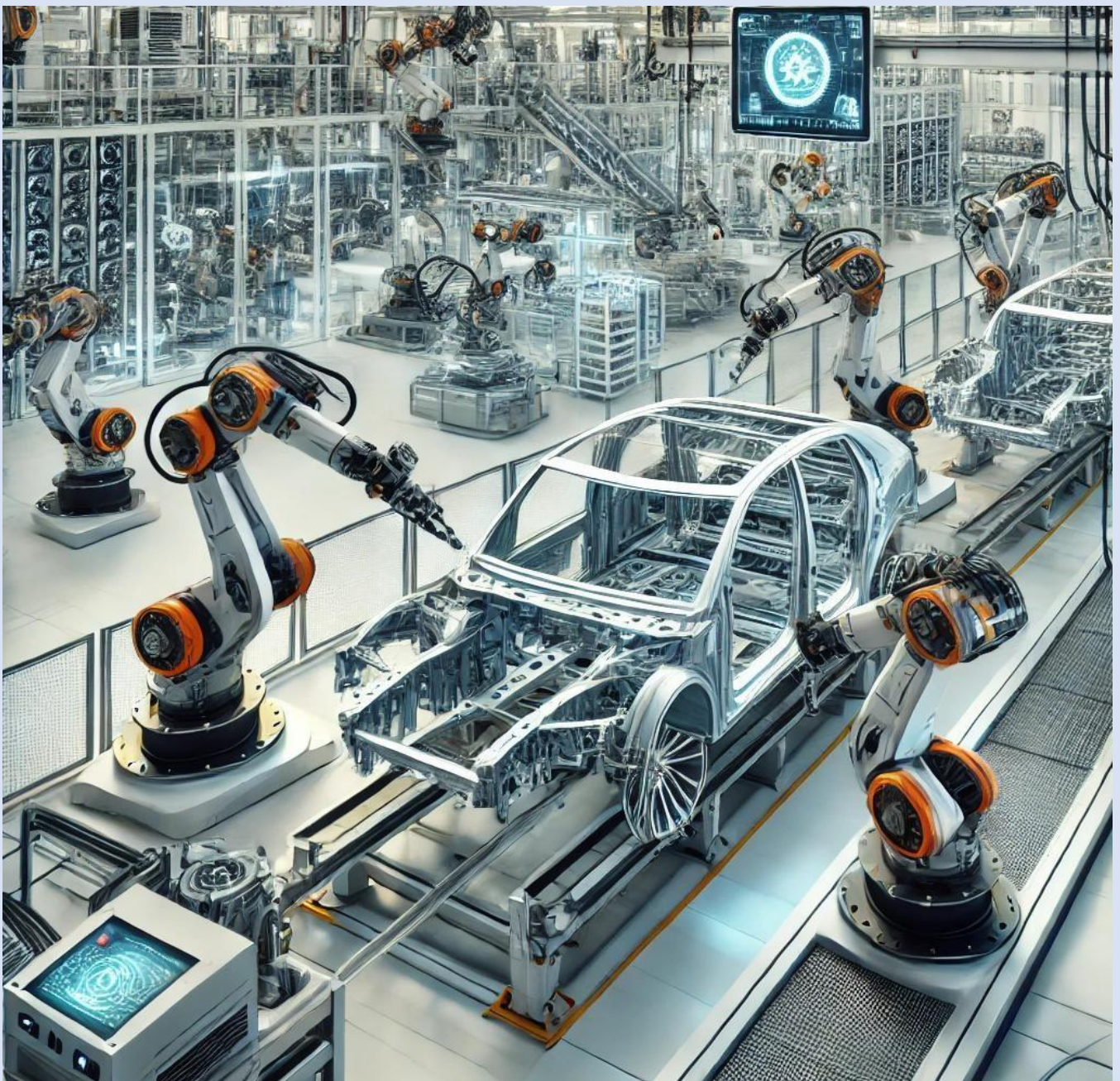
Technologia i Automatykacja Montaży
Assembly Techniques and Technologies

TIAM

Technologia i Automatykacja Montaży

Open Access: journals.prz.edu.pl/tiam • e-ISSN-2450-8217 • Volume 126, Issue 4, 2024

Publisher: Łukasiewicz Research Network – Warsaw Institute of Technology • Rzeszow University of Technology • Patronage SIMP • Since 1993



**RZESZOW UNIVERSITY
OF TECHNOLOGY**



Łukasiewicz
Warsaw Institute of Technology

CONTENTS

3

Iga Barca, Jan Godzimirski, Marek Rośkowicz

Strength tests of repair joints loaded with tension and loss of stability

Badania wytrzymałości węzłów naprawczych obciążonych na rozciąganie i utratę stateczności

14

**Andrzej Wojciech Stępnikowski,
Andrzej Zbrowski**

E-learning, VR and techno-educational stands as a way for practical optimisation of education for the automation needs

E-learning, VR oraz stacje techno-dydaktyczne jako praktyczna optymalizacja edukacji dla potrzeb automatyki

19

Ewelina Ozga, Władysław Zielecki

The influence of aging on the load capacity of adhesive lap joints made of aluminum alloy EN AW-2024-T3

Wpływ starzenia na nośność połączeń klejowych zakładkowych ze stopu aluminium EN AW-2024-T3

28

**Izabela Miturska-Barańska, Michał Bornus,
Rafał Szadura**

Analysis of the possibilities of implementing alternative methods of joining semfinished products in the production process of steel rims

Analiza możliwości wdrożenia alternatywnych metod łączenia półwyrobów w procesie produkcji felg stalowych

37

Lidia Gałda

Surface topography creation of machine elements after carburizing process with application of burnishing method

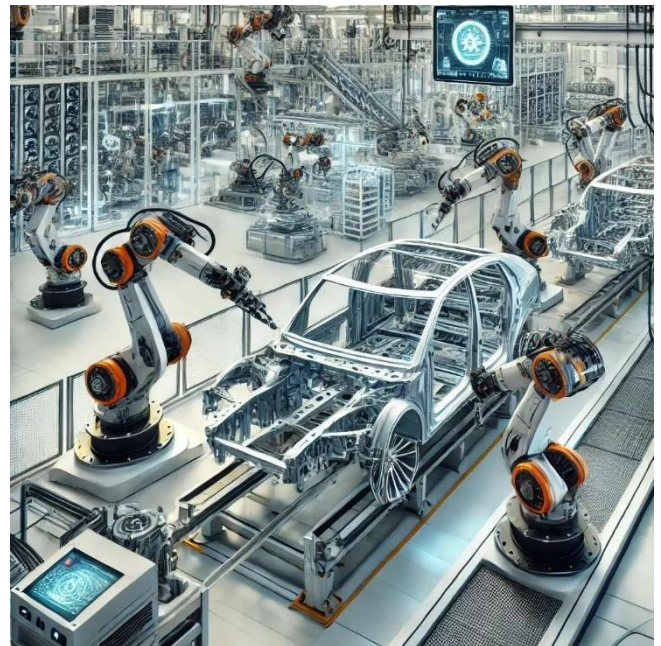
Kształtowanie topografii powierzchni elementów maszyn po nawęglaniu z wykorzystaniem metody nagniatania

44

Jan Czyżewski

Voice control system for collaborative robot used in assembly process

System sterowania głosem dla robota kolaboracyjnego wykorzystywanego do procesu montażu



Quarterly „Technologia i Automatykacja Montaży” is listed on the list of scored journals of Polish Ministry of Education and Science - 40 points.

STRENGTH TESTS OF REPAIR JOINTS LOADED WITH TENSION AND LOSS OF STABILITY

BADANIA WYTRZYMAŁOŚCI WĘZŁÓW NAPRAWCZYCH OBCIĄŻONYCH NA ROZCIĄGANIE I UTRATĘ STATECZNOŚCI

Iga BARCA^{1,*} , Jan GODZIMIRSKI¹ , Marek ROŚKOWICZ¹ 

¹ Faculty of Mechatronics, Armament and Aerospace, Military University of Technology, Warsaw, Poland

* Corresponding author: iga.barca@wat.edu.pl

Abstract

During aircraft service, the skin is the component that first comes into contact with factors that can cause mechanical damage - that is why it is most often damaged during use. Semi-monocoque aircraft structures are made of a skin and a frame. The skin is an element that significantly affects the safety of the structure, since it transfers loads between the elements of the frame. For this reason, the skin is subject to special supervision during technical maintenance, and any damage detected must be repaired. The research was carried out on specimens made of AW 2024-T3 plate sheet with a thickness of 1 mm. In the study, a comparative analysis of damaged, undamaged and repaired specimens loaded in tension and compression was performed. Different patches were used in repaired specimens, made of metallic as well as composite materials, connected to the structure with rivets or using adhesive materials. The study showed that the use of riveted as well as adhesively bonded overlays does not allow the original strength of the tensile-loaded skin to be restored, but does allow the strength of the compression-loaded skin to be restored. In addition, numerical simulations were performed to define the stress field occurring in the adhesive joint for different geometric dimensions of the plate. The results of the numerical analysis showed that the geometry of the plate model influences the values of reduced stresses in the adhesive weld and the patch. Regardless of the analyzed changes in the geometry of the plate model, the maximum values of reduced stresses are similar to each other. The smallest values of reduced stresses in the adhesive joint and composite patch were obtained for the case of a plate with a thickness of 1 mm and a width of 160 mm.

Keywords: repair node, semi-monocoque structure, composite materials, numerical calculations

Streszczenie

Podczas eksploatacji statków powietrznych pokrycie jest elementem, który w pierwszej kolejności ma kontakt z czynnikami mogącymi wywołać uszkodzenie mechaniczne – stąd najczęściej ulega uszkodzeniu podczas eksploatacji. Konstrukcje półskorupowe statków powietrznych wykonane są z pokrycia i szkieletu. Pokrycie jest elementem, który istotnie wpływa na bezpieczeństwo konstrukcji, ponieważ przenosi obciążenia pomiędzy elementami szkieletu. Z tego powodu pokrycie podlega szczególnemu dozorowi podczas przeglądów technicznych, a wykryte uszkodzenia muszą być naprawione. Badania prowadzono na próbkach wykonanych z arkusza blachy AW 2024-T3 o grubości 1 mm. W pracy wykonano analizę porównawczą próbek uszkodzonych, nieuszkodzonych i naprawionych próbkach obciążonych na rozciąganie i ściskanie. W próbkach naprawianych zastosowano różne nakładki, wykonane z materiałów metalowych jak i kompozytowych, łączonych ze strukturą nitami lub z wykorzystaniem tworzyw adhezyjnych. Badania wykazały, że zastosowanie nakładek nitowanych jak i klejonych nie umożliwiają odtworzenia pierwotnej wytrzymałości pokrycia obciążonego na rozciąganie, ale umożliwiają odtworzenie wytrzymałości pokrycia obciążonego na ściskanie. Dodatkowo wykonano symulacje numeryczne, w celu zdefiniowania pola naprężeń występujących w spoinie klejowej dla różnych wymiarów geometrycznych płyty. Wyniki analizy numerycznej wykazały, że geometria modelu płyty wpływa na wartości naprężeń zredukowanych w spoinie klejowej i nakładce. Niezależnie od analizowanych zmian w geometrii modelu płyty maksymalne wartości naprężeń zredukowanych są do siebie zbliżone. Najmniejsze wartości naprężeń zredukowanych w spoinie klejowej oraz nakładce kompozytowej otrzymano dla przypadku płyty o grubości 1 mm i szerokości 160 mm.

Słowa kluczowe: węzeł naprawczy, konstrukcja półskorupowa, kompozyt, obliczenia numeryczne



1. Introduction

Semi-monocoque structures have been a common design solution for aircraft airframes for many years (Motley, 1980). Semi-monocoque designs are made of a skin and a frame, and both the frame and the skin carry the loads caused by external forces (Hoff, 1946). In the past, in beam structures, the skin was made of fabric (Akash et al., 2017; Al-Rabeei, 2024), and at that time it was not as important structural element as modern skin made of aluminum alloys or composite materials (Azmin et al., 2012).

The formula of semi-monocoque structure can be used to make wings, fuselage or aircraft aileron, and the strain on these elements is caused by the presence at the same time shearing forces, bending moments and torsional moments, which consequently cause a complex state of stress, in the elements of the frame and in the skin (Siddiqui, 2014; Kołodziejczyk and Święch, 2018). In particular, the aircraft skin is the component that first comes into contact with factors that can cause mechanical damage to the structure – thus it is most often damaged during aircraft life (Cantwell and Morton, 1992; Henaff et al., 2019).

Making repairs to the skin is an important aspect that affects the safety of the structure, since the skin is also a component that transfers loads between framing members, including stringers, spars and ribs. Damage to the skin impacts to the stress distribution in the skin itself, but also in the adjacent framing elements and in the connections occurring between the skin and the frame. The consequence of primary damage to the skin can be further propagation of damage to adjacent elements and secondary damage. For this reason, the skin is particularly subject to supervision during technical inspections (Bazargan, 2010), and detected damage to the skin must be repaired to maintain its integrity and restore the original strength of the damaged component (Chang and Zang, 2023; Armstrong et al., 2005; Dai et al., 2020).

Repairs of metallic aircraft structures using composite materials and adhesive materials were initiated in 1970 (Baker, 1984; Baker 1999; Baker and Joned, 1988). It is not a widely used method in the repair of metallic aircraft structures, due primarily to the challenges associated with the certification process. However, considering: the favorable time-consumption of the adhesive repair process (practically defined by the crosslinking time of structural adhesive materials), the durability of the repair and, above all, the lack of the need for additional secondary damage (mounting holes), repairs of aircraft structures using composite patches and adhesive bonds are still being developed. (Hamill and Nutt, 2018; Rośkowitz and Smal, 2012).

The classic solution for installing repair patches is to use mechanical fasteners in the form of, for example, rivets (Camanho and Lambert, 2006). The main disadvantage of this type of solution, as previously mentioned, is the additional local “weakening” of a section of the undamaged skin by making mounting holes (Camanho and Matthews, 1999). However, based on research, it has been shown that repairs using adhesive materials have a number of advantages over the traditional repair method in which mechanical fasteners are used, such as lighter weight, more streamlined shape, ability to reproduce more complicated shapes, reduction of stress concentration around the repair node (Ma et al., 2021, Megueni and Yala, 2009) and effective load transfer especially in thin-walled parts (Ayedi et al., 2014, Gan et al., 2006). Repair of skin elements can be made by cutting a hole in the shape of a circle, triangle, rectangle, trapezoid, ellipse and octagon. At the site of the damage, after removing a section of the skin, an insert reproducing the cut hole can be installed in the made hole, and a patch is installed to ensure the tightness of the repair node and restore locally the strength and stiffness parameters of the damaged element (Barca and Rośkowitz, 2022).

Publication (Khazaei et al., 2021) analyzed the effect of the patch material used on the restoration of the original strength of the repaired structure, and publication (Bond and Maxwell, 1999) studied the effect of the type of repair used with symmetrical and asymmetrical composite patches on the stress intensity factor during fatigue testing. The study showed that the type of symmetric and asymmetric patches used significantly affects the fatigue life of the repaired metal plate.

Other publications (Prakash et al., 2013; Albedah et al., 2021; Lee et al., 2021; Gunnion and Wang, 2009) analyzed the effect of the applied patch shapes in the repair node on the values of the stress intensity factor. It was shown that its greatest decrease occurred with octagonal-shaped patches, and that the use of an elliptical patch shape reduces the amount of material removed compared to a circular shape by up to 41% in the repaired structure, and results in a reduction in shear stress in the structure of up to 18% compared to a cut-out circular shape (Shazly, 2021).

So far, there has been a lot of work on performing adhesive repairs using composite materials for the repair of metal skin, semi-monocoque aircraft structures. The publication (Katnam et al., 2013) reviews previous research and analysis on the possibility of using composite materials in primary aircraft structures. The issue of using composite materials in the repair of aviation structures is complicated, if only because of the anisotropic properties of composite

patches or the different, depending on their location in the aircraft structure, dominant loads on the same elements. An example of such an element is the wing skin, which is in tension at the bottom of the wing and compression at the top of the wing.

Therefore, the purpose of this work is to perform a comparative analysis of undamaged, damaged and repaired specimens loaded in tension and compression. The repaired specimens used various patches, made of both metallic and composite materials, connected in the repair zone traditionally with rivets or bonded to the repair nodes with adhesive materials. On the occasion of the realization of comparative studies, numerical simulations were carried out with the aim of defining the stress field occurring in the adhesive joint, that is, in the element most important for the restoration of the original strength and stiffness properties of the skin damage zone (Achour et al., 2013). The main aim was to test the possibilities of repairing metal thin skins of semi-monocoque aircraft structures by applying composite patches.

2. Research methodology

Comparative tests of repair junctions were carried out on specimens made of EN AW2024-T3 aluminum alloy with a 20 mm diameter hole (representation of the so-called small punctures of the skin). The geometric dimensions of the used specimens are presented in Figure 1. Metal inserts also made of EN AW2024-T3 aluminum alloy with a diameter of 20 mm were riveted to the previously prepared repair pads (metal and composite) with a diameter of 70 mm using a rivet $\phi 1.5$ mm of PA 25 alloy.

Three types of material were used for composite patches made of:

- Aeroglass 110g/m² glass fabric made from 10 layers with $[0^\circ;45^\circ]_5$ orientation infused with L285/H285 resin in mass proportions of 100:40 - the obtained patch thickness was equal to 1 mm (GFRP – Glass Fiber Reinforced Polymer);
- carbon composite made by the company (Silesian Science and Technology Center of Aviation Industry Sp z o.o. from 10 layers of GG204T 2x2 Twill 3K prepreg with $[0^\circ;45^\circ]_5$ orientation - the resulting overlay thickness was equal to 1.6 mm (CFRP – Carbon Fiber Reinforced Polymer);
- EN AW-2024-T3 aluminum alloy plates with thicknesses of 0.3, 1 and 2 mm.

The 70 mm diameter patches were bonded to the specimen using adhesives: DP 420 (3M USA) and Loctite 9464 (Henkel Germany). Adhesive materials were selected on the basis of in-house tests, the results

of which were presented in the publication (Barca et al., 2023). The surfaces to be bonded were grinded with 3M abrasive discs of 80 grit. As reference specimens, riveted specimens with patches were also prepared, using 6 rivets of 3.5 mm diameter made of PA 25 aluminum alloy. The geometry of the specimen and the rivet joint is shown in Figure 2. The mounting holes were made with a 3.5 mm drill bit at an angle of 90°. The holes were made at a distance of 10 mm from the edge of the patch. The angle between the holes is 60°. Variants of the fabricated specimens are shown in Table 1 and Figure 3.

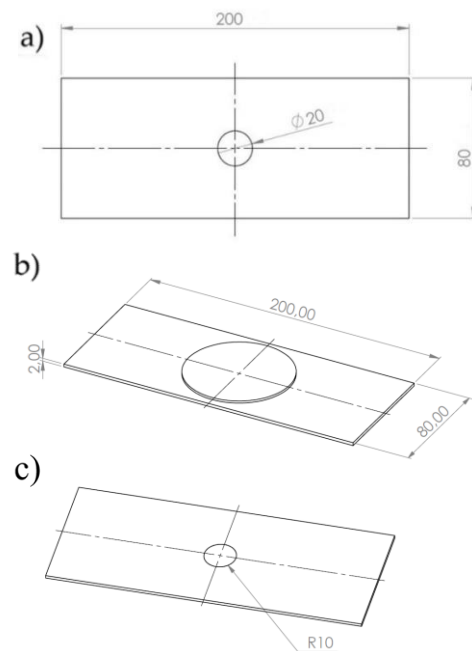


Fig. 1. Geometric dimensions: a) plate with hole, b) repaired specimen (patch $\phi 70$ mm), c) repaired specimen (second side with insert $\phi 20$ mm)

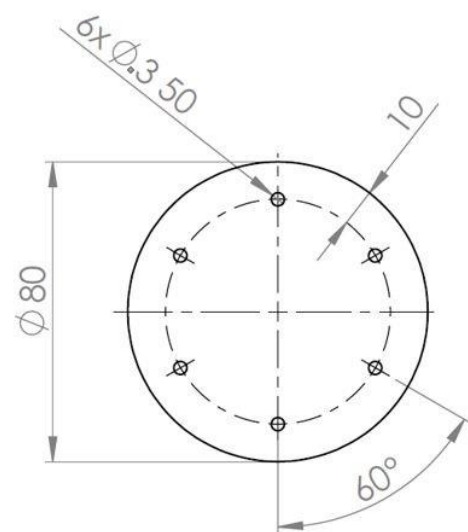
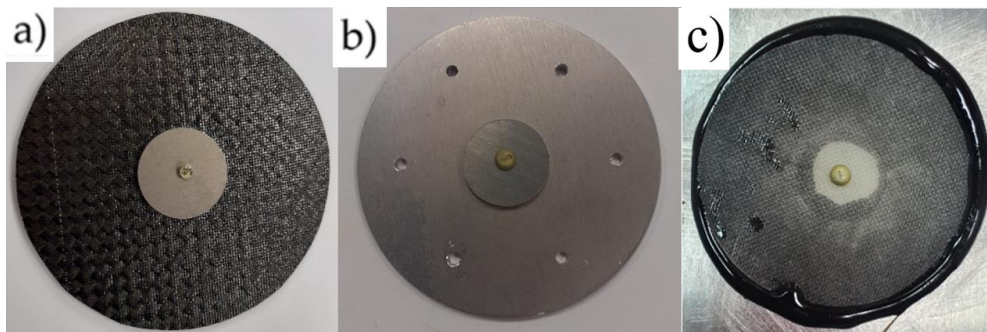


Fig. 2. Geometry of the rivet joint

Table 1. Variants of the specimens made

Specimen No.	Patch material	Patch diameter [mm]	Patch thickness [mm]	Type of patch connection
1.	AW-2024-T3	80	2	mechanical /rivets
2.			2	adhesive /DP 420
3.			1	adhesive /DP 420
4.			0.3	adhesive /DP 420
5.	CFRP	70	1.6	adhesive /DP 420
6.			1.6	adhesive /Loctite 9464
7.	GFRP	70	1	adhesive /Loctite 9464
8.			1	adhesive /DP 420

**Fig. 3.** Prepared patches: a) CFRP, b) aluminum alloy, c) GFRP

The specimens were subjected to tensile and compression tests. Static tests were carried out on a Fritz Heckert ZD10 testing machine at a speed of 2 mm/min. Tensile specimens were fixed in flat jaws, while compression specimens were supported articulated on both sides by placing them in the prismatic grooves of the testing machine's platters. The values of the failure forces for the tension-loaded specimens and the critical force during loss of stability for the compression specimens were recorded.

3. Results and discussion

3.1. Tensile test results

The results of the static tensile tests performed on specimens with repair nodes. For each case, three specimens were tested, the obtained force values of which were averaged and placed in a Table 2. Examples of the failure forms of the tested specimens are shown in Figure 4. In specimens with bonded patches, specimen cracking was observed in the section weakened by the hole. In the case of specimens with riveted patch, damage propagation began at the location of holes prepared for rivets.

Table 2. Tensile test results

Specimen No.	Specimen type	Patch			Force [kN]
		Material	Thickness [mm]	Patch connection type	
1	Undamaged	-	-	-	69.3
2	Damaged	-	-	-	50
3	Repaired	AW-2024-T3	2	mechanical /rivets	46.3
4			2	adhesive /DP 420	49.5
5			1	adhesive /DP 420	53.8
6			0.3	adhesive /DP 420	53
7		CFRP	1.6	adhesive /DP 420	51.2
8			1.6	adhesive /Loctite 9464	50
9		GFRP	1	adhesive /Loctite 9464	50
10			1	adhesive /DP 420	49.5

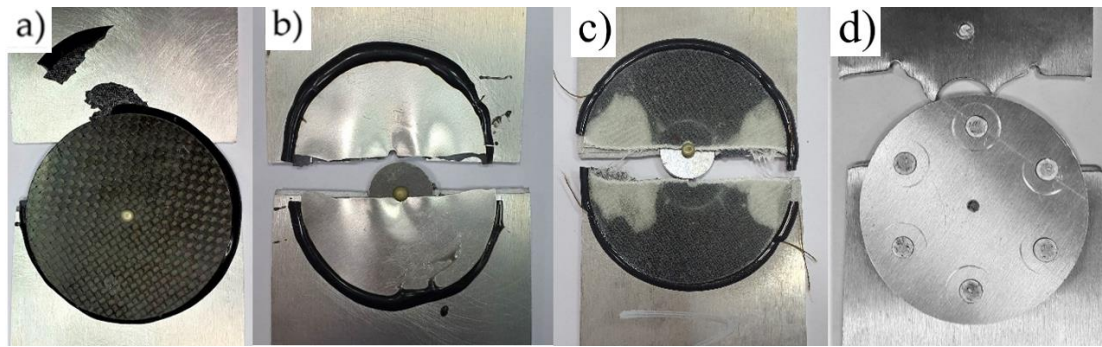


Fig. 4. Photos of failure of tensile specimens with overlay: a) carbon, b) metal thickness = 0.3 mm, c) glass, d) riveted metal thickness = 2 mm.

The form of damage with a hole was related not only to the reduction of the loaded cross-sectional area by the 20 mm diameter hole, but also resulted from the occurrence of the phenomenon of stress concentration in the area of the rivet mounting holes. The failure stresses in the specimen without a hole are:

$$\sigma_n = \frac{F}{A} = \frac{69300}{80 \times 2} = 433 \text{ MPa} \quad (1)$$

While a in a specimen with a hole:

$$\sigma_{no} = \frac{F}{A} = \frac{50000}{60 \times 2} = 416.7 \text{ MPa} \quad (2)$$

The effect of stress concentration at a 20-mm-diameter hole causes a slight decrease in strength of about 4% when the material is deformed in the plastic range. The repair methods used practically did not increase the tensile strength of the specimens. The consequence of the classical repair performed with riveted overlays was a reduction in the failure load of the specimen because the rivet holes as so-called stress concentrators were the places from where the failure process of the specimen probably started (Fig. 4d). When the specimens with stiffer patches (CFRP and AW-2024-T3 with a thickness of 2 mm) were loaded and in the load range of about 30 kN, “crackling” was heard due to the cracking of adhesive joints and the

patches themselves did not fail (Fig. 4a). Overlays with lower stiffness (glass composite and AW-2024-T3 with a thickness of 0.3 mm) decohered simultaneously with the repaired specimen (Fig. 4b, Fig. 4c).

3.2. Compression test results

The manner of deformation of the specimens during the compression test is shown in Figure 5. The results of the static compression tests carried out on the specimens with repair nodes. Again, three specimens were tested for each case, and the resulting force values were averaged and placed in a Table 3.



Fig. 5. Specimen loaded with compressive force

Table 3. Results of compression test of specimens

Specimen No.	Specimen type	Patch				Force [kN]
		Material	Diameter [mm]	Thickness [mm]	Patch connection type	
1	Undamaged	-			-	0.75
2	Damaged	-			-	0.7
3	Repaired	AW-2024-T3	80	2	mechanical /rivets	1.18
4			70	2	adhesive /DP 420	1.2
5		CFRP		1.6	adhesive /DP 420	1.53
6				1.6	adhesive /Loctite 9464	2.2
7		GFRP		1	adhesive /Loctite 9464	1.95
8			1	adhesive /DP 420	0.95	

Assuming that the test specimens loaded axially along the dominant geometric dimension, behave as jointed supported bars, the critical force value for the undamaged specimen was calculated.

$$F_{critical} = \frac{\pi^2 E \times J}{l^2} \quad (3)$$

$$J = \frac{b \times h^3}{12} = \frac{80 \times 2^3}{12} = 53.3 \text{ mm}^4 \quad (4)$$

$$F_{critical} = \frac{\pi^2 70000 \times 53.3}{210^2} = 835 \text{ N} \quad (5)$$

The calculated value of the critical force for the specimen without a hole was greater than the experimentally defined value by 10%.

The critical force for the specimen with the hole was about 7% less than the critical force of the undamaged specimen. Each of the repair methods used resulted an increase in the critical force of the repaired specimens compared to the critical force of the undamaged specimen. In specimens with a CFRP patch bonded with DP 420 adhesive (Figure 6a), plastic deformation of the specimen material outside the repair node occurred during loading - what meant that the repair node excessively stiffened the specimen in the repair zone. Plate deformation in plastic range outside the patch. In the case of large deformations of the loaded specimen, failure of the adhesive bond also occurred, but only when the repair patch was on the tensile side during bending of the specimen. (Figure 6b, Figure 7).

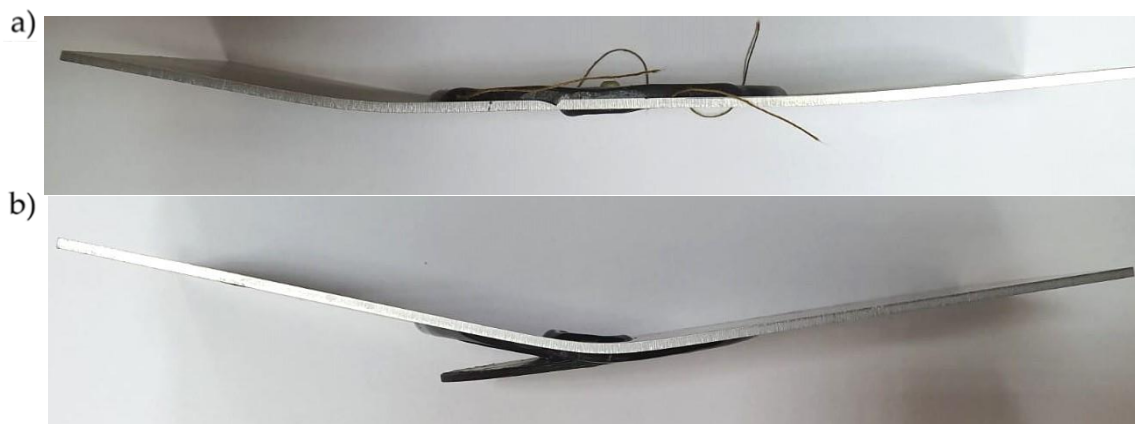


Fig. 6. Failure mode of specimens with CFRP patch: a) permanent deformation outside the repair node, b) failure of the adhesive joint

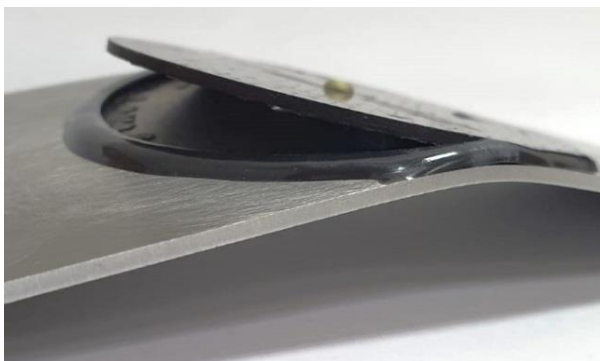


Fig. 7. Plastic deformation of the plate with CFRP patch after loss of stability (failure of the adhesive joint)

The riveted patch specimen plastically deformed upon loss of stability (the deflection arrow was about 1.4 mm, but the riveted joint did not fail. The overlay made of 1 mm thick glass composite did not deform after the loss of stability of the loaded specimen. The patch deformed with the specimen without being damaged.

4. Numerical simulations

Using the finite element method and the computational capabilities of the CAE environment Ansys Workbench 2021R2 Static Structure module, the effect of the specimen geometry (its thickness and width) on the stress distributions occurring in the plate, patch and adhesive joint was analyzed. The calculations took into account the nonlinear properties of the AW-2024-T3 aluminum alloy by assuming a multilinear model of the material. The material constants of the DP 420 adhesive were determined experimentally during static tensile testing of the adhesive, Figure 8. Based on the $\sigma = (\sigma)\epsilon$ curve of the DP 420 adhesive, the multilinear material properties of the adhesive were defined (Table 4). The nonlinear properties of AW 2024 T3 alloy are shown in Table 5. The properties of the composite material (GFRP) was defined as orthotropic with parameters presented in Table 6.

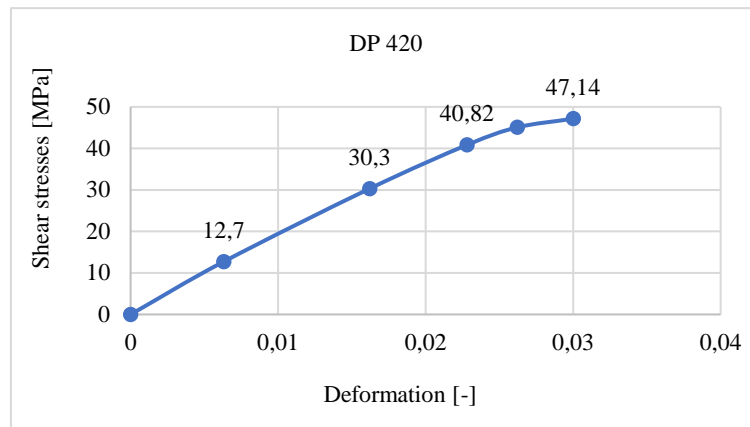


Fig. 8. $\sigma = (\sigma)\epsilon$ curve of DP 420 adhesive

Table 4. Strength parameters of DP 420 adhesive

Name of material	Young's modulus [GPa]	Poisson's ratio [-]	Strain [-]	Stress [MPa]
DP 420	2.083	0.35	0	1
			0.0063	12.7
			0.0162	30.3
			0.0228	40.82
			0.0262	45.05
			0.03	47.14

Table 5. Strength parameters of AW 2024 T3 aluminum alloy (Godzimirski and Pietras, 2012)

Name of material	Young's modulus [GPa]	Poisson's ratio [-]	Strain [-]	Stress [MPa]
AW 2024T3 NL	70	0.36	0	330
			0.0098	348.45
			0.0196	370
			0.0385	410.8
			0.0741	468.72
			0.1071	507.36
0.1379	540.56			

Table 6. Orthotropic properties of the composite patch

Name of material	Young's modulus [GPa]			Poisson's ratio [-]			Kirchhoff module [GPa]		
	X	Y	Z	XY	YZ	XZ	XY	YZ	XZ
GFRP	15	15	5	0,04	0,3	0,3	3	2,2	2,2

Simulations were carried out for four design cases.

Case I – the geometric dimensions of the plate model were the same as the samples used in the experimental tests (Figure 9). The model was of an element of dimensions 150x80x2 mm (length, width, thickness) with a hole of 20 mm diameter. The defined specimen was shorter than the specimen used in the experiment due to the skip of the specimen surface located in the jaws of the testing machine - Figure 10. An insert with dimensions equal to the diameter of the hole was modeled in the hole. An adhesive joint with a diameter of 70 mm and a thickness of 0.15 mm and a composite patch with a diameter of 70 mm and a thickness of 1.6 mm were also modeled.

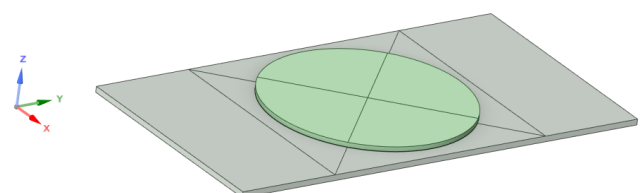


Fig. 9. The model of the repair node in the Geometry module

Using the *Contacts* function, the types of contacts occurring between the various elements of the model were defined. *Frictional* contacts with a factor of 0.1 were defined between the insert and the plate. *Bonded* contacts were defined between the adhesive joint and

the patch, the adhesive joint and the plate, and the adhesive joint and the insert [27].

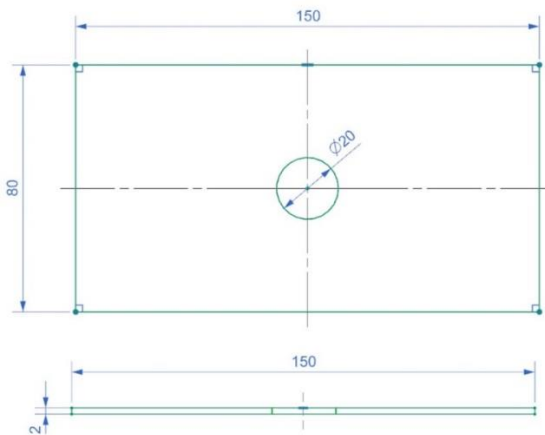


Fig. 10. Dimensions of the repaired plate

Discretization of the model was performed using the *Mesh* function. In the mesh parameters for the entire model, the *Mesh* elements were given a size of 2 mm. In order to obtain a hexagonal mesh, the *Multizone* function was used, defining the properties of a *Hexa*-type mesh. The *Edge Sizing* function was also used, and an element size of 1 mm was set on the edge of the hole. After the geometry was discretized, a model consisting of 4289 elements and 31162 nodes of Hex20 type was obtained.

Case II – The thickness of the plate was reduced from 2 mm to 1 mm. The plate had the following geometric dimensions: 150x80x1 mm (length, width, thickness);

Case III – the width of the plate was increased from 80 mm to 160 mm. The plate had the following

geometric dimensions: 150x160x2 mm, (length, width, thickness);

Case IV – The width of the plate was increased from 80 mm to 160 mm and its thickness was reduced from 2 mm to 1 mm. The plate had the following geometric dimensions: 150x160x1 mm - (length, width, thickness).

In each case, the thickness of the composite patch was equal to 1.6 mm. Loads were defined by assuming that the stresses in the undamaged cross-section of the repaired panel should be equal to 220 MPa, which resulted from the yield strength of the material equal to 330 MPa and taking into account the safety factor equal to 1.5. Based on the value of the cross-section of each case, the maximum force was determined - Table 7.

Table 7. Load values for design cases

Case No.	Force kN
I	35.2
II	17.6
III	70.4
IV	35.2

The boundary conditions of the simulation were similar to those of the experimental test specimens - Figure 11. One edge of the model was fixed using *Displacement* ($D_x, D_y, D_z = 0; R_x, R_y, R_z = \text{Free}$), the opposite edge was fixed using *Displacement* ($D_z = 0, D_y, D_x = \text{Free}; R_x, R_y, R_z = \text{Free}$) and the tensile *Force* was modeled with the values shown in Table.

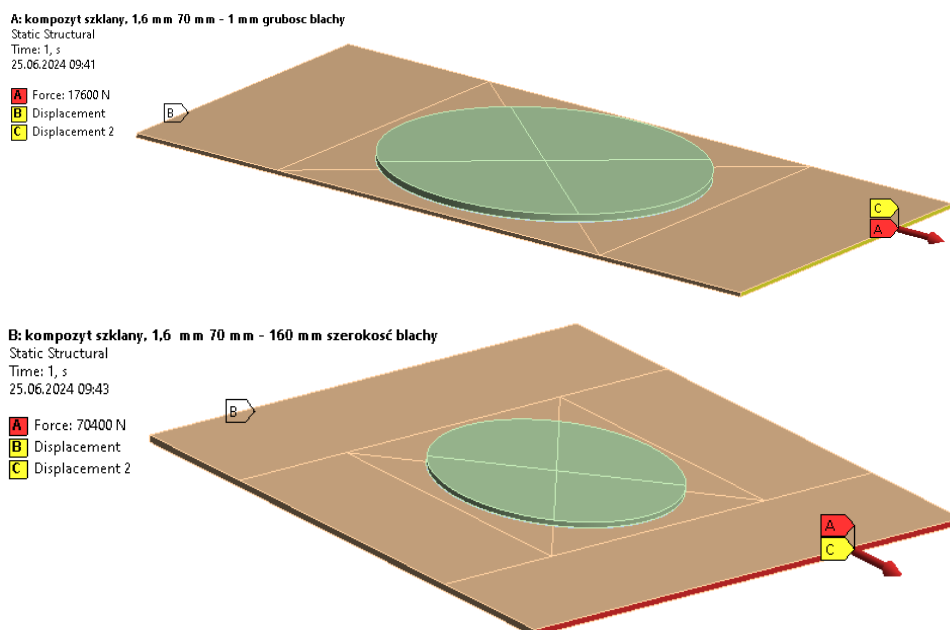


Fig. 11. Geometry and boundary conditions of case I and III

Example maps of reduced stresses according to the Huber-M-H hypothesis in plates for the four design cases are presented in Figures 12, 13, 14, 15, while

Table 8 shows a summary of the maximum values of reduced stresses in the elements of the repair node.

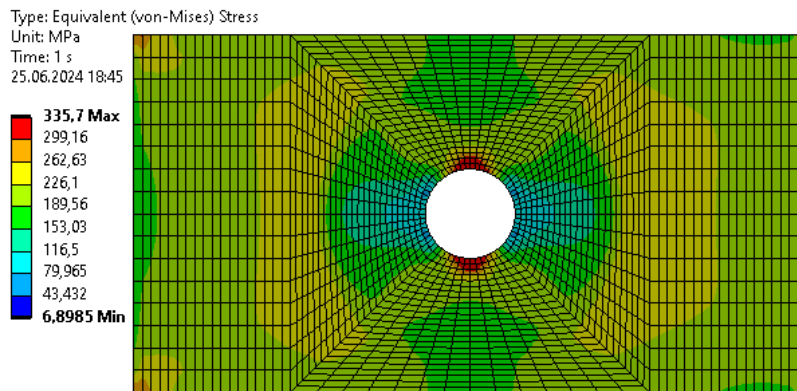


Fig. 12. Von-Mises stress map (Case I)

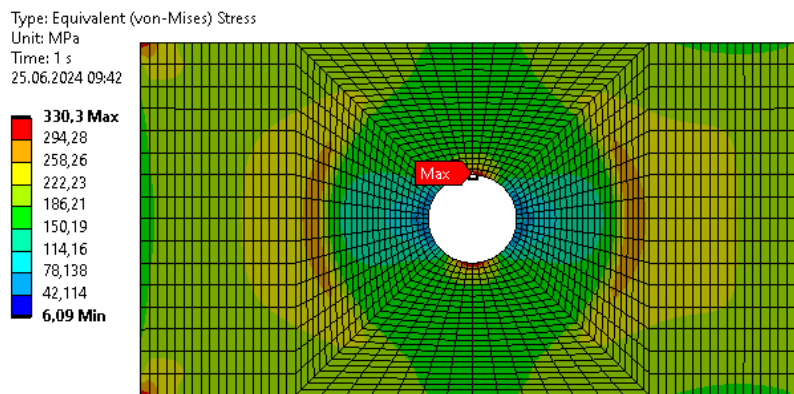


Fig. 13. Von-Mises stress map (Case II)

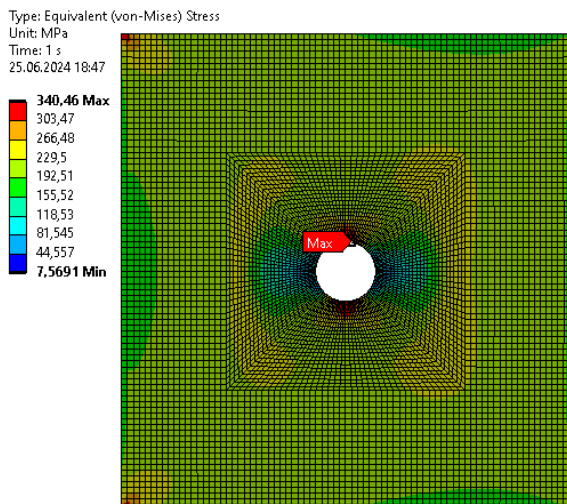


Fig. 14. Von-Mises stress map (Case III)

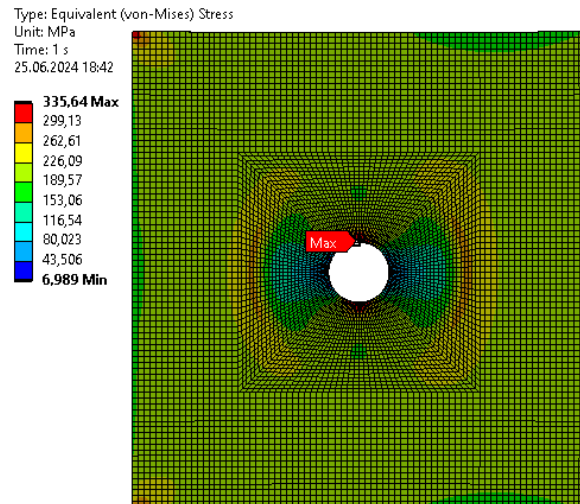


Fig. 15. Von-Mises stress map (Case IV)

Table 8. Results of numerical simulations of repair nodes

Calculation cases	Force kN	Maximum values of reduced stresses (von-Mises) [MPa]		
		Plate	Patch	Adhesive
Thickness 2 mm, width 80 mm	35.2	336.53	164.65	47.14
Thickness 1 mm, width 80 mm	17.6	334.48	92.35	30.44
Thickness 2 mm, width 160 mm	70.4	340.46	125.35	38.63
Thickness 1 mm, width 160 mm	35.2	335.64	98.36	30.74

The results of the numerical analysis show that the geometry of the model has an impact on the values of reduced stresses in both the adhesive joint and the patch. Significant differences in stress values are found in the composite patch (44%) and the adhesive joint (35%). Regardless of the analyzed changes in the geometry of the plate model, the maximum values of reduced stresses (according to the Huber -M-H hypothesis) in the repaired model are very close to each other (differences at the 1% level).

Taking into account the values of adhesive bond failure stresses of modern adhesive bonding materials, it follows that it is rational to repair thin metal skin by bonding composite patches. The positive effect of reducing stresses in adhesive joints was also observed for the case when the area of the repair zone is smaller in relation to the total area of the repaired specimen.

5. Conclusions

Based on experimental studies, it was concluded that:

- repairs using both riveted and bonded patches do not allow the restoration of the original tensile strength of the loaded skin, but allow the restoration of the compressive strength of the loaded skin (loss of stability);
- for elements of the skin where tensile loads on the material dominate, such as the lower part of the wing skin, stiffer patches (of greater thickness (1mm, 2 mm) or made of materials with higher stiffness - carbon-epoxy composite) should be used. It allows to reduce the stress level by 7.6% compared to the damaged one;
- for compression elements where loss of stability may occur, such as the upper part of the wing skin, patches with lower stiffness (thinner or, for example, made of glass-epoxy composite) are better.

The results of the numerical tests showed that:

- it is reasonable to repair only thin metal coverings by bonding composite patches due to the maximum stresses in the adhesive joints;
- there can be a reduction of stresses in the adhesive joints (35%) when the area of the repair node is smaller in relation to the total area of the repaired zone.

Acknowledgments

Funding: This work was financed by Military University of Technology under research project UGB 735/2024.

References

- Achour T., Aid A., Albedah A., Bouanani M.F., Benyahia F., Bouiadja B., Belhouari M., (2013). *Materials and Design* 50, 433-439.
- Akash B., Apiccella A., Aversa R., Petrescu R., Bucinell R., Corchado J., Petrescu F. (2017). History of aviation - a Short review. *Journal of Aircraft and Spacecraft Technology*. 1 (1), 30-49.
- Al-Rabeei S., Korba P., Hovanec M., Sekelová I., Kale U. (2024). Structural design and material comparison for aircraft wing box beam panel. *Heliyon*. Volume 10, Issue 5.
- Albedah A., Bouiadja B.A.B., Bouiadja B.B., Benyahia F., Mohammed S.M.A.K., Mhamdia R. (2021). Fatigue crack growth in aluminum panels repaired with different shapes of single-sided composite patches. *Int. J. Adhes. Adhes.* 105, 102781.
- Armstrong KB., Cole W.W., Bevan G. (2005) Care and repair of advanced composites. SAE International.
- Ayedi H.F., Guermazi N., Haddar N., Elleuch K. (2014). Investigations on the fabrication and the characterization of glass/epoxy, carbon/epoxy and hybrid composites used in the reinforcement and the repair of aeronautic structures. *Materials*. 56, 714-724.
- Azmin Shakrine, Prince Hasn, Mohd Rafie, Fairuz Izzuddin Romli. (2012). Modern design trend of metal aircraft fuselage structure. *International Science Postgraduate Conference 2012*. Volume 808-817.
- Baker A. (1984). Repair of cracked or defective metallic aircraft components with advanced fibre composites – an overview of Australian work. *Composite Structures*. Volume 2, Issue 2, 153-181.
- Baker A., Joned R. (1988). Bonded Repair of Aircraft Structures, *Martinus Nijhoff Publishers*.
- Baker A. (1999). Bonded composite repair of fatigue-cracked primary aircraft structure. *Composite Structures*. Volume 47, Issue 1-4, 431-443.
- Barca I., Rośkiewicz M. (2022). Analysis of the airframe repair node. *Assembly Techniques and Technologies*. 3/2022, 42-48.
- Barca I., Godzimirski J., Rośkiewicz M. (2023). Selection of materials for repairing punctures of metal skin of semimonocoque structures using composite patches.

- Assembly Techniques and Technologies*. Volume 120, Issue 2/2023, 19-32.
- Bazargan M. (2010). Airline operation and scheduling. *Ashgate Publishing Limited*, Farnham.
- Bond D., Davis M. (1999). Principles and practices of adhesive bonded structural joints and repairs. *International Journal of Adhesion and Adhesives*. Volume 19, Issues 2-3, 91-105.
- Chang R.C., Zang S. (2023). Structure health inspection for aging transport aircraft. *Aircraft Engineering and Aerospace Technology*.
- Camanho P.P., Matthews F.L. (1999). A progressive damage model for mechanically fastened joints in composite laminates. *Journal of Composite Materials*. 33 (24), 2248-2280.
- Camanho P.P., Lambert M. (2006). A design methodology for mechanically fastened joints in laminated composite materials. *Composites Science and Technology*. 66 (15), 3004-3020.
- Cantwell W.J., Morton J. (1992). The significance of damage and defects and their detection in composite materials: a review. *The Journal of Strain Analysis for Engineering Design*, 27 (1), 29-42.
- Dai J.T., Zhao P.Z., Su H.B., Wang Y.B. (2020). Mechanical Behavior of Single Patch Composite Repaired Al Alloy Plates: Experimental and Numerical Analysis. *Materials*. 13, 2740.
- Gan, Salehi-Khojin, Zhamu; Zhong. (2006). Effects of patch layer and loading frequency on fatigue fracture behavior of aluminum plate repaired with a boron/epoxy composite patch. *J. Adhes. Sci. Technol.* 20, 107-123.
- Godzimirski J., Pietras A. (2012). Numerical strength analysis of hybrid sandwich composites. *WAT Bulletin*. Vol. LXI, Nr 3.
- Gunnion A.J., Wang C.H. (2009). Optimum shapes of scarf repairs. *Composites Part A Applied Science and Manufacturing*, 40 (9), 1407-1418.
- Hamill L., Nutt S. (2018). Adhesion of metallic glass and epoxy in composite-metal bonding. *Composites Part B: Engineering*. Volume 134, 186-192.
- Henaff G., Renon V., Larignon C., Perusin S., Villechaise P. (2019) Identification of Relationships between Heat Treatment and Fatigue Crack Growth of alpha beta Titanium Alloys. *Metals*. 9, 512.
- Hoff N.J. (1946). A Short History of the Development of Airplane Structures. *Journal Article*. Volume 34, No. 3, 370-388.
- Katnam K.B., Da Silva L.F.M., Young T.M. (2013). Bonded repair of composite aircraft structures: A review of scientific challenges and opportunities. *Progress in Aerospace Sciences*. Volume 61, 26-42.
- Khazaei M., Mohammadi S., Yousefi M. (2021). A review on composite patch repairs and the most important parameters affecting its efficiency and durability. *J. Reinf. Plast. Compos.* 40, 3-15.
- Kołodziejczyk R., Świąch Ł. (2018). Mechanics in Aviation ML-XVIII 2018 Stiffness study of thin-walled composite wing structure of unmanned aircraft. *Polish Society for Theoretical and Applied Mechanics*.
- Lee H., Seon S., Park S., Walallawita R., Lee K. (2021). Effect of the geometric shapes of repair patches on bonding strength. *J. Adhes.* 97, 207-224.
- Ma L., Zhou W., Ji X., Yang S., Liu J. (2021). Review on the performance improvements and non-destructive testing of patches repaired composites. *Composite Structures*. 263, 113659.
- Megueni A., Yala A.A. (2009). *Materials and Design*. 30(1), 200-205.
- Motley George Ronald. (1980). A Study Of The Reinforcement Required For Cutouts In Aircraft Semi-monocoque Structure. *Southern Methodist University ProQuest Dissertations & Theses*. 8012578.
- Prakash M.B., Ramji M., Srilakshmi R. (2013). Towards optimization of patch shape on the performance of bonded composite repair using FEM. *Compos. Part B Eng.* 45, 710-720.
- Rośkiewicz M., Smal T. (2012). The use of composite materials to repair of aircraft semi-monocoque aircraft semi-monocoque airframes. *ECCM15 – 15th European Conference on Composite Materials*.
- Shazly Mostafa. (2021). Improvement of scarf repair patch shape for composite aircraft structures. *The Journal of Adhesion*. 1044-1070.
- Siddiqui Tariq. (2014) Aircraft Materials and Analysis. *McGraw Hill Education*. Page 9.

E-LEARNING, VR AND TECHNO-EDUCATIONAL STANDS AS A WAY FOR PRACTICAL OPTIMALISATION OF EDUCATION FOR THE AUTOMATION NEEDS

E-LEARNING, VR ORAZ STACJE TECHNO-DYDAKTYCZNE JAKO PRAKTYCZNA OPTIMALIZACJA EDUKACJI DLA POTRZEB AUTOMATYKI

Andrzej Wojciech STEPNIKOWSKI¹ , Andrzej ZBROWSKI¹ 

¹ Łukasiewicz Research Network – Institute for Sustainable Technologies, Kazimierza Pułaskiego 6/10, 26-600 Radom, Poland

* Corresponding author: andrzej.stepnikowski@itee.lukasiewicz.gov.pl

Abstract

The publication presents a hybrid learning approach for training in the field of automation, focused on Programmable Logic Controllers and teacher-trainer relation in the VR. In this case hybrid learning is a mix of such methods like: physical techno-educational stands (possible to be used also for distant learning), e-learning courses and Virtual Reality Learning Environment (VRLE). In this article we will present two such VRLE that can be used through web browsers 2D and/or fully immersive experience in VR. To some extent we will present here also results of our initial research on the use of VR in this context. This article gives an insight on the ways how to embed such interactive environment with traditional forms like work-based learning, simulations and e-learning courses. Such “blended” education helps to develop learning management system through the Protocol of Learning Technologies Integration (PLTI). This contribution presents results of studies conducted during hybrid workshops in Poland and Lithuania. Results show that blended learning approach can give greater motivation and satisfaction to a learner thanks to multi-modal learning environment (MMLE), moreover there are some indications that it could also enrich learning retency. This MMLE was developed in response to market demands (pilot), offered and implemented in research laboratories by the Ruhr University in Bochum (Germany) and Łukasiewicz Institute for Sustainable Technologies in Radom (Poland). Such actions are aligned with the newly adopted EU strategy to lead Web 4.0 and virtual worlds.

Keywords: Vocational Education and Training (VET), PLC, hybrid and blended learning, Virtual Reality, digital twins

Streszczenie

Publikacja przedstawia wyniki badań porównawczych prowadzonych nad zastosowaniem hybrydowych metod nauczania w obszarze automatyki z orientacją na programowanie sterowników PLC i szkolenie-trenerów w VR. W tym kontekście hybrydowe nauczanie stanowi zestaw metod takich, jak: fizyczne stanowiska techno-dydaktyczne (z możliwością prowadzenia nauki zdalnie), kursy e-learningowe i środowisko edukacyjne wirtualnej rzeczywistości (SEWR). W niniejszym artykule zaprezentowano dwa SEWR, gdzie dodatkowo autorzy rozwiązań przewidzieli możliwość nauczania w aplikacji desktopowej - poza VR. Publikacja prezentuje także wyniki pierwszych badań w zakresie używania gogli VR w kontekście edukacji zawodowej. Artykuł daje wgląd w metodykę nauczania z zastosowaniem zarówno nowoczesnych form interaktywnych, jak i bardziej tradycyjnych opartych na uczeniu się w miejscu pracy, symulacjach i e-learningu. Takie „mieszane” podejście do edukacji pozwala stworzyć system zarządzania procesami nauczania i dalszej optymalizacji, dzięki tzw. Protokołowi Integracji Technologii w Edukacji (PITE). Autorzy prezentują wyniki badań przeprowadzonych podczas warsztatów hybrydowych w Polsce i na Litwie. Wyniki badań pokazują, iż mieszane podejście może w większym stopniu przelożyć się motywację i satysfakcję dla uczestnika dzięki Multi-modalnemu Środowisku Edukacyjnemu (MMSE), co więcej pojawiły się wskazania świadczące, iż tak prowadzony proces może pozytywnie wpłynąć na poziom retencji uczenia się. To multi-modalne podejście powstało w oparciu o zapotrzebowanie rynku (pilotaż) i nawiązaną w ramach projektu

współpracę laboratoriów badawczych Uniwersytetu Zagłębia Ruhr z Bochum w Niemczech i Łukasiewicz-Institut Technologii Eksploatacji w Radomiu. Badania weryfikacyjne prowadzono w Kolegium Koweńskim na Litwie, a w ich efekcie dopracowano założenia kursu e-learningowego i przygotowano założenia pod kolejny projekt dotyczący wirtualizacji stanowiska techno-dydaktycznego do nauki programowania robotów z przeznaczeniem do pracy w systemach inspekcji wizyjnej. Warto zwrócić uwagę, iż tego typu inicjatywy wpisują się w nowo przyjętą Strategię UE w zakresie Web 4.0 i wirtualnych światów.

Słowa kluczowe: kształcenie zawodowe, sterowniki PLC, hybrydowe i mieszane formy kształcenia, wirtualna rzeczywistość, cyfrowe bliźniaki

1. Introduction

On 11th July 2023 European Commission has adopted a new strategy on Web 4.0 and virtual worlds to steer the next technological transition. Four key strategy pillars of this strategy were indicated. Two of them are about empowering people, reinforcing skills and supporting an European Web 4.0 industrial ecosystem. Strategy states that specialists in virtual worlds are essential and stakeholders should cooperate to set up a talent pipeline and support further skills development. European citizen's panel has provided 23 recommendations including those on human-centricity, education, awareness-raising and skills on how to use Virtual Worlds. This is a strong signal that modern and comprehensive learning paths with combined methods and VR are needed, especially in the leading branches like automation and machinery, automotive, food processing, chemistry and energy where Programmable Logic Controllers (PLC) are widely used (IRA, 2021, pp.5). PLCs are mostly used in the automation and machinery sector (79%), so in above mentioned context, it is crucial to improve ways to prepare industry professionals for the challenges of digital transformation and Industry 4.0. This is even more important in RIS (Regional Innovation Scheme) countries like Poland, Lithuania or Slovakia.

That is why project PLC-Centered VR-training for Industry 4.0 was developed (VR-PLC). In that project existing training PLC techno-educational stand was augmented and virtualized as we have created a digital twin of technological transport stand. Together with German colleagues we have developed a virtual simulator of a physical simulator. Upskilling with the use of such digital twin in Virtual Learning Environment is supported by 2D version, hybrid workshops (to test tools) and e-learning course delivered by European Institute of Innovation and Technology (EIT Manufacturing) via Skillsmove.eu platform.

The aim of this project was to design attractive way of learning with the use of elements of

gamification and microcredentials (digital badges) admitted by EIT-M. Thanks to use of gamification learners gain the feeling of control, feedback, sense of achieving goals and feeling of progress (Świtalski W., Łódź 2019).

Our institute was previously involved in the development of other VR Learning Environment (VLE) while leading Erasmus+ project called "Collaborative VR Platform for e-learning: Teaching Communication". Two VR rooms were created with adoption of some classrooms functionalities like: screen for presentation, whiteboard, sticky notes, etc. (Stępnikowski A.W., ed. 2023). Due to those experiences we had a chance to implement new EIT-M project in 2023 called PLC-centered VR-Training for Industry 4.0: Train the trainer enabling interaction mode between teacher/trainer and the trainee. In addition we have also put a virtualized visual inspection robot arm to the techno-educational stand. Such innovative, highly accessible VR-PLC platform can empower workers and reinforce skills enabling acquisition of vocational and digital skills.

The rationale for carrying out the project was the need for optimization of the up- and re-skilling of VET and higher education students (I phase) and professionals (II phase) and make easier access to education for adults. Another reason was to disseminate digitalization processes in companies (ia. in Poland only 11% of companies are highly digitalized compared to an average of 26% in the EU). Such solutions will be also delivered by Mazovia EDIH project consortium (Łukasiewicz-ITEE is a partner there).

The results of the project – after validation workshops in Kaunas College and AGH University of Kraków - met a positive feedback, especially with regard to motivation and insight into functionalities of PLC programming, some remarks were given also in the context of teaching and previous experiences with VR in the educational context.

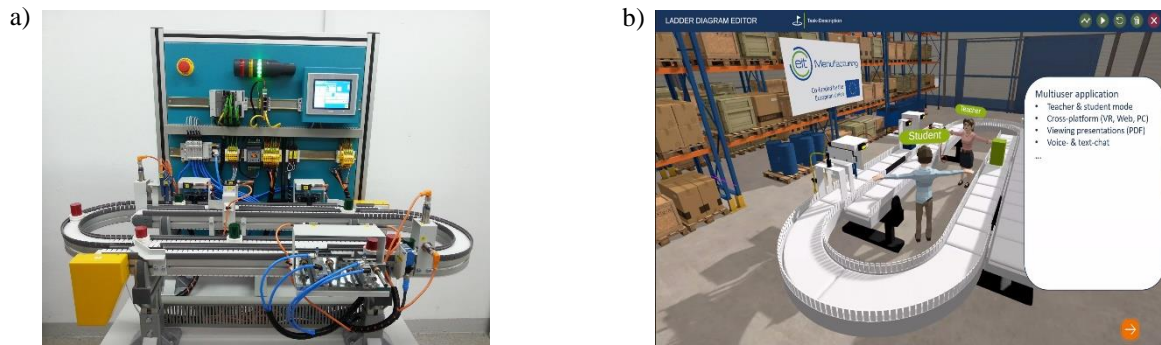


Fig. 1. Examples of VR-PLC functionalities: a) physical stand, b) digital twin in the VR Learning Environment

2. The concept of the blended learning with the use of VLE

The multilevel concept of the holistic remote training of PLC programming was founded already a few decades ago. Initially the main idea was to deliver a simulator (techno-education stand) to program the physical device in a chosen language and see how it reacts and moves in real-time. It was also about demonstration how relatively low costs of the training are and such stands were produced for VET and teaching centers. When the remote mode was enabled, it was possible to program the machine without actual presence of a trainee. That was also case at our Institute as we have developed few such stands for robotics and learning ladder diagram. After a few years it appeared that this concept can be further developed with other solutions like e-learning course (PLC languages, basic and advanced instructions, etc.) and VR technology (Fig. 2). In terms of functionality, such blended approach offers greater attractiveness and accessibility which contributes to a better learning retention level. This also allows to reduce travel time, cost and impact on the environment. In 2023 additional modules were developed in order to prepare VR-PLC trainers – both in Skillsmove.eu e-learning course (leadership, interculturality, teaching methods, etc.) and in VLE. Each module can be also certified in this learning platform after finishing a learning path (each one includes several learning nuggets). Such learning platform reflects a competence and could be understood as a microcredential and/or electronic badge.

Theoretical knowledge serves as an introduction and shows broader contexts. Skillsmove.eu platform also provides on-line tests for instant feedback on knowledge acquisition alternating with 3D experiences for practical use of gained knowledge. Learning paths and virtual training have passed the EIT-Manufacturing quality control process to ensure professional adequacy. The main VLE functionalities are:

- adequate virtualization of a physical stand,
- access to a simplified version to perform most basic tasks with a limited number of sensors and actuators,
- possibility to be used in the desktop version through a web browser – WebGL 2.0 standard (mouse and keyboard are used so no VR headset is needed). That gives possibility to be used by people with problems with VR motion sickness,
- learner's progress in particular levels of VLE is recorded and sent back to the supporting learning platform where it is marked as completed in the system,
- in 2023 an multi-axis robotic arm for visual inspection was added (to show some more functionalities),
- an avatar of a trainer also has appeared enabling more interactive and engaging way of learning.

There are several engaging elements of the VLE as learners can interact with the digital stand, view supporting texts and get familiar with actuators and sensors, i.e. by blocking a light barrier with their hand. Set of those methods we call multi-modal learning environment (MMLE).

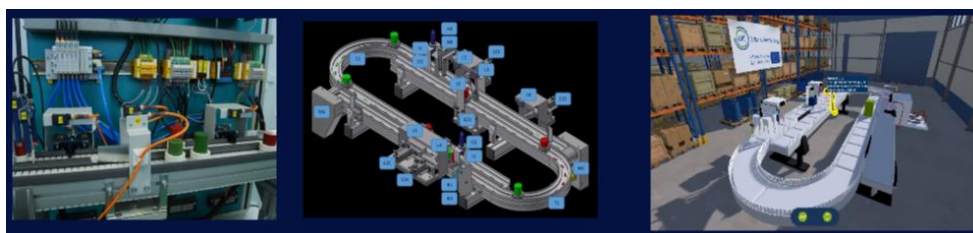


Fig. 2. Visualisation of blended learning approach (physical, HMI and VR)

3. Implementation and conducted research

In the beginning of 2022 Łukasiewicz-ITEE and LINPRA (Lithuanian Association of Industry Engineers) have conducted a survey for managers from metal-machinery and automotive industries with regard to training needs and methods (n=16). Only 16% of participants (namely from two companies) were experiencing training with the use of VR while 64% of asked medium- and high-level managers indicated that it would be an interesting offer. There were also some differences even between countries here as in Poland e-learning was mentioned as more used form that in the Lithuania (77% vs 58%). 1/3 of respondents stated that it takes too much effort to go to the training. Last but not least, the less desired educational form were long-lasting formal vocational upskilling conducted for over 1 year (Stępnikowski A.W. 2022).

Bearing that in mind, during two years of our projects 39 unique learning nuggets were developed in three languages: English, Polish and Lithuanian (resulting in 89 nuggets in total structured in 17 learning paths). Based on the assumptions of the previously tested program for physical stand in the e-learning platform we have added other elements such as: digital twins, PLC learning languages, basic and advanced instructions, function blocks and an introduction to robot programming. Additionally there are “educational” nuggets for trainers of trainers like: training methods and forms in VR, trainer personalities, training cycle, diversity and sustainability aspects. This context of sustainability for the use of VR and AR was elaborated i.a. based on the developments of research on the effectiveness of training on professional maintenance (X-Wei L., et al., 2022). The Learning Management System (LMS) Moodle was used while VR elements were planned for Oculus Quest 2 standalone. As it was mentioned few levels of practical tasks in the field of programming were also developed in the VLE (Fig. 3). Those theoretical and practical elements were developed and tested during physical workshops and training in Radom, Kaunas, Kielce, Lublin and Krakow (over 100 learners and about 30 teachers and VET trainers).



Fig. 3. Virtualization of the ladder diagram programming

Here are results of research conducted by us in Lithuania in 2022 and 2023. They were submitted to EIT-M as these effects were part of the final report. First pilot workshop took place on October 2022 in Kaunas Kolegija (Lithuania) with 40 participants (HE students from robotics and automation faculty and industry managers). A survey was conducted and in its results VLE was indicated as an easy tool to be used (55%) with intuitive user interface (60%) and VR experiences felt realistic (50%). For most of respondents (80%) it was easy to navigate in the environment. This workshop was successful thanks to showing different options of learning PLC programming. Those learners however – in general – as students did not feel prepared to work on real PLCs, which also might be a result of an (over)simplification of the VLE. The second Lithuanian workshop took place in 2023 and was dedicated to VET and higher education teachers and trainers/instructors. It was a verification of the methods of programming but also of train-the-trainer module. Research survey was conducted among participants (n=26). It appeared that most of them were satisfied with the content, interactions and outcomes of a workshop (75%), similar number of participants were assessing VR experiences positively (70%). Fewer positive opinions were given on e-learning content (60%) and that could be also due to the fact that nuggets in Lithuanian language were still in the revision phase. 60% of participants see a potential in the use of VR in VET training and it is worth to mention that only 25% of them had previous experiences with VR. It is interesting to compare respondents indications on the usability of VR in the VET training, namely:

- 65% indicates that they could be used for training on complex machines;
- 60% states that VR could be useful in the maintenance and repair simulations (training sessions for maintenance tasks);
- 60% indicates that it could be used widely for training of individuals geographically dispersed;
- 55% state that it could be used for simulation of high-risk scenarios;
- 45% indicates that VR could be used for virtual labs experiments (chemical or physical experiments in controlled VLE);
- 40% states that VR is a good tool for real-time feedback and assessment;
- 25% indicates that VR could be used for soft skills training (e.g. communication and leadership).



Fig. 4. Pictures from the Lithuanian workshop in 2022 and visualization of the VLE

4. Conclusions

In accordance with the new strategy on Web 4.0 and virtual worlds to steer the next technological transition, research organisations need to build support for skills development for virtual worlds at regional and national levels while EIT's role is to boost EU's virtual technological capacity. It is worth to remind that "re-skilling" is one of four main pillars of this strategy. VR-PLC project with its continuation (train-the-trainer) was contributing to this policy. The main goal of the concept was to virtualize existing technological stand of a technological transport in order to foster skills acquisition on PLC programming by blending learning methods. Authors are presenting hybrid workshop with the use of VLE and Skillsmove.eu e-learning platform. Two validation workshops conducted in Lithuania by researchers from our institute and Ruhr University of Bochum have confirmed that mix of learning methods is the good way to support learning process (70% shared positive opinions). Each element (short lecture, physical stand, e-learning, VLE) has covered other PLC programming aspects. Emphasis was placed on different aspects of PLC and it have received positive feedback from the most of 66 participants (75%). This overall results were a function of quality of trainers work and program content with strong focus on the originality level and intensity of the transmission - including dynamics adapted to participants feelings and expectations (Stępnikowski A.W. ed., 2023, pp. 55). Trainers were innovative Meta VR Trainers (Sałata E., Bojanowicz S. eds. 2017). Participants were not so enthusiastic about e-learning course (54%) – due to translation problems and some lacking functionalities. Those issues were solved after pilot workshops.

During all of those events in Lithuania and Poland each time a few people felt dizzy due to the motion

sickness in VR (ca. 5-10%). This problem is less experienced while sitting, yet longer periods of time (over 15-20 minutes) in VLE increases the likelihood of that risk. After 30 minutes learner should take a break. That is also an important obstacle in wider dissemination of VLEs as they should to be supported by other methods, preferably hybrid. New opportunities are rising - especially for maintenance training - with the use of AR.

References

- Sałata E., Bojanowicz J. (eds.), *Kształcenie nauczycieli do funkcjonowania w zmieniającej się rzeczywistości edukacyjnej. Teoria i praktyka*, Uniwersytet Humanistyczno Techniczny im. K. Pułaskiego, Radom 2017.
- Siewert J.L., Wolf M., Trientsios P., Gerhard D., Integrated blended learning approach for PLC training in industry 4.0 with web-based and VR experiences, Lecture notes in networks and systems, *LNNS*, volume 763.
- Stępnikowski A.W., Virtual Reality learning retention in education and training, *Journal of Continuing Education*, Łukasiewicz-ITEE, 4(115), Radom 2021.
- Stępnikowski A.W. (ed.), *COViR Teachers' Guide*, Łukasiewicz-ITEE, Radom 2023.
- Świtalski W., *Uczenie się dorosłych w zabawie*, Wydawnictwo Uniwersytetu Łódzkiego, Łódź 2019.
- Liu X-W., Li C-Y., Dang S., Wang W., Qu J., Chen T., Wang Q-L., Research on training effectiveness of professional maintenance personnel based on Virtual Reality and Augmented Reality Technology, Sustainability, *MDPI* 2022, 14(14351) <https://doi.org/10.3390/su142114351>.
- An EU initiative on Web 4.0 and virtual worlds: a head start in the next technological transition, European Commission Recommendation, COM(2023) 442.
- European Citizens' Panel on Virtual Worlds. Final Report, Luxembourg: Publications Office of the European Union, 2023.
- Informator Rynkowy Automatyki, edycja 2021, Automatyka, podzespoły, aplikacje, AVT-Korporacja, Warszawa 2021.

THE INFLUENCE OF AGING ON THE LOAD CAPACITY OF ADHESIVE LAP JOINTS MADE OF ALUMINUM ALLOY EN AW-2024-T3

WPLYW STARZENIA NA NOŚNOŚĆ POŁĄCZEŃ KLEJOWYCH ZAKŁADKOWYCH ZE STOPU ALUMINIUM EN AW-2024-T3

Ewelina OZGA^{1,*} , Władysław ZIELECKI¹ 

¹ Department of Machines Technology and Production Engineering, Faculty of Mechanical Engineering and Aeronautics, Rzeszów University of Technology, Powstańców Warszawy 12, Rzeszów, Poland

* Corresponding author: e.guzla@prz.edu.pl

Abstract

The aim of the study was to assess the effect of environmental ageing on the load capacity of single-lap adhesive joints made of EN AW-2024-T3 aluminum alloy, subjected to and not subjected to pneumatic shot peening. Adhesive joints were made using two-component epoxy adhesive Loctite EA 3430. Half of the formed joints were strengthened by pneumatic shot peening of the overlap zone. The shot peening time was 120 s, the ball diameter was 1.0 mm, and the compressed air pressure was 0.5 MPa. The adhesive joints were then subjected to different variants of ageing in natural conditions. Individual variants differed in the length of ageing. The next step was to examine the load capacity of the adhesive joints using a static tensile test. The results were subjected to statistical analyzes, including analysis of variance (ANOVA), regression and correlation analysis, and Student's t test. Based on the analyzes, it was found that for the assumed range of input factor variability, ageing of joints not subjected to shot peening increased their load capacity by 38%. Aging of joints strengthened by shot peening resulted in a 62% decrease in their load capacity. The ageing length had a significant effect on the load capacity of the adhesive joints.

Keywords: adhesive joints, aging, shot peening, strengthening of adhesive joints

Streszczenie

Celem pracy była ocena wpływu starzenia środowiskowego na nośność połączeń klejowych jednozakładkowych ze stopu aluminium EN AW-2024-T3, które poddano i nie poddano procesowi pneumokulkowania. Połączenia klejowe wykonano z użyciem dwuskładnikowego kleju epoksydowego Loctite EA 3430. Połowę utworzonych połączeń umocniono za pomocą pneumokulkowania strefy zakładki. Czas pneumokulkowania wynosił 120 s, średnica kulek 1,0 mm, a ciśnienie sprężonego powietrza 0,5 MPa. Następnie, połączenia klejowe poddano różnym wariantom starzenia w warunkach naturalnych. Poszczególne warianty różniły się długością starzenia. Kolejnym krokiem było zbadanie nośności połączeń klejowych za pomocą statycznej próby rozciągania. Uzyskane wyniki poddano analizom statystycznym, które obejmowały przeprowadzenie jednoczynnikowej analizy wariancji ANOVA, analizy regresji, korelacji i testu t-Studenta. Na podstawie przeprowadzonych analiz stwierdzono, że dla przyjętego zakresu zmienności czynników wejściowych, starzenie połączeń niepoddanych pneumokulkowaniu, zwiększyło ich nośność o 38%. Starzenie połączeń umocnionych w procesie pneumokulkowania spowodowało natomiast zmniejszenie ich nośności o 62%. Długość starzenia miała istotny wpływ na nośność połączeń klejowych.

Słowa kluczowe: połączenia klejowe, starzenie, pneumokulkowanie, umacnianie połączeń klejowych

1. Introduction

Adhesive joints are exposed to many factors that can affect their strength and durability. Awareness of

the existence of such factors and knowledge of the potential effects of their impact are crucial from the point of view of designing safe adhesive joints.



The mechanical properties of adhesive joints can be significantly affected by daily and annual fluctuations in temperature and air humidity. Water can cause changes in the physical and mechanical properties of the adhesive as well as damage the bonds between the adhesive and the adherend (Bowditch, 1996). The results of the analyzes that examine the effect of moisture on adhesive joints by immersing them in water indicate that the negative impact of the aquatic environment on the adhesive joint increases with increasing exposure time and water temperature (Hirulkar et al., 2020).

Another degrading factor may be the ambient temperature. As a result of long-term exposure to elevated temperatures (e.g., in the summer season), the adhesive undergoes the so-called thermal degradation. In the first stage of degradation, the mechanical strength of the joints increases as a result of the additional crosslinking of the adhesive structure. However, in the later phase of the process, excessive crosslinking of the adhesive structure occurs or its molecular weight is reduced. As a result, the strength of the joints decreases (Rojek, 2011).

The phenomenon of increasing the strength of the joints in the first phase of the degradation process can be used to strengthen the adhesive joints. It has been shown that the additional heating of joints during curing has a beneficial effect on their static strength at both ambient and elevated temperature (Szabelski et al., 2016). It has been proven that the strength of adhesive joints increases as a result of their aging at high temperature (150-200°C). The authors of the study associated the improvement of strength properties with additional crosslinking of the adhesive structure and reduction of stress concentration resulting from uneven polymerization shrinkage on the bonded surfaces (Morcos et al., 2022). The improvement in strength properties was also obtained as a result of the aging of adhesive joints subjected to cyclic daily and annual temperature fluctuations in natural conditions or in a thermal shock chamber (Zielecki et al., 2021).

Another factor that should be considered when designing adhesive joints is the possibility of using additional procedures to increase their strength. Methods of strengthening adhesive lap joints include, among others: rounding the edge zone of the lap (Çalık, 2016, Zhao, 2011), narrowing the ends of the lap (Belingardi, 2002), creating steps in the lap area (Durmuş, 2019), making an undercut along the edge of the adhesive joint (Bahrami, 2019), sandblasting (Godzimirski, 2018) or pneumatic shot peening of the lap zone (Zielecki, 2008, Ozga, 2023).

Pneumatic shot peening of the lap zone is one of the simplest and most affordable methods of

strengthening adhesive joints. As a result of this procedure, the adherend is deformed, and compressive stresses are created in the bond line. The introduced stresses are added to the stresses coming from the external (shearing) load. As a result, the degree of stress concentration in the edge zone of the bond line is reduced and the strength of the joint is increased. It has been shown that as a result of pneumatic shot peening, the strength of adhesive overlap joints made of S235JR steel can be increased by as much as 93-112% (Zielecki, 2008).

To sum up, the literature analysis indicates that exposing adhesive joints to elevated temperatures may have a beneficial effect on their strength properties. The load capacity of the adhesive joints can also be increased by pneumatic shot peening of the overlap zone. However, the impact of ageing on the load capacity of adhesive joints subjected to pneumatic shot peening has not been investigated so far. Therefore, the objective of the research presented in the article is to determine the effect of environmental ageing (daily and annual fluctuations in temperature and air humidity) on the load capacity of adhesive joints subjected to and not subjected to the pneumatic shot peening process.

2. Material and methods

2.1. Preparation of adhesive joints

The subject of the study was single-lap adhesive joint made of the EN AW-2024-T3 aluminum alloy designated according to PN-EN 485-2+A1:2018-12 standard. Due to its good fatigue resistance, this alloy is used, among others, in the aviation and military industries, for example, in landing gear structures and wing tensioning elements. This alloy is not suitable for welding and anodizing. It is characterized by low corrosion resistance and good workability (Dobrzański, 2012, PN-EN, 2018-12).

The adhesive joints were made using the two-component epoxy adhesive Loctite EA 3430 (Loctite, Düsseldorf, Germany). This is a general-purpose adhesive. It cures quickly at room temperature. Increasing the ambient temperature also shortens the curing time (Technical Data Sheet, 2024). Table 1 presents the physical properties of the Loctite EA 3430 adhesive.

The first stage of the process was to prepare the adherend surfaces. In order to properly develop the geometric structure, the surfaces were subjected to abrasive blasting with 95A electrocorundum with a grain size of 0.27 mm using a New-Tech sandblasting cabinet (New-Tech, Wrocław, Poland). The values of the roughness parameters, measured using a Taylor Hobson SURTRONIC 25 contact

profilometer (Taylor Hobson Ltd, Leicester, England) were: $R_z = 25.95 \mu\text{m}$, $R_a = 4.53 \mu\text{m}$, $R_q = 5.67 \mu\text{m}$, $R_{Sm} = 0.141 \text{ mm}$, $R_{ku} = 2.99$ (average values determined based on the measurements carried out for 6 randomly selected samples). The measurements were carried out in accordance with the standard PN-EN ISO 21920-2:2022-06. After mechanical processing, the bonded surfaces were degreased with acetone.

Table 1. Selected Physical properties of Loctite EA 3430 adhesive

Physical properties ¹		
Property	Unit of measurement	Value
Coefficient of thermal conductivity	W/(m·K)	0.3
Tensile strength	N/mm ²	36
Tensile modulus	N/mm ²	3 210
Compressive strength	N/mm ²	65
Elongation	%	2
Shore hardness, (durometer D)		70
Glass transition temperature	°C	58

¹ Cured for 7 days at a temperature of 22 °C; 1.2 mm thick samples.

The next stage was to create adhesive joints. The adhesive components were mixed manually in a 1:1 ratio, in accordance with the manufacturer's recommendations. After the components were mixed, a small amount of the adhesive composition was applied to adherend surfaces and spread using a triangular comb device. This made it possible to evenly distribute the composition on the surface and remove excess of the composition to obtain the appropriate thickness of the bond line. The elements with the applied layer of adhesive were placed in a fixing device. The device ensured the achievement of the appropriate dimensional and shape accuracy of the adhesive joints, prevented the movement of the elements, and allowed for exerting even pressure on the constituted adhesive joint using one-kilogram weights. The application of pressure allowed for better filling of micropores and micro-irregularities of the surface, facilitating the spreading of the adhesive and the fixing of the joined elements. When selecting the weight of the weights, care was taken to avoid excessive leakage of the adhesive between the bonded surfaces or deformation of the structure. The constant amount of adhesive, its viscosity, and the constant pressure force determined the thickness of the adhesive joint, which was 0.09 ± 0.01 mm. A simplified scheme of adhesive joints is shown in Fig. 1.

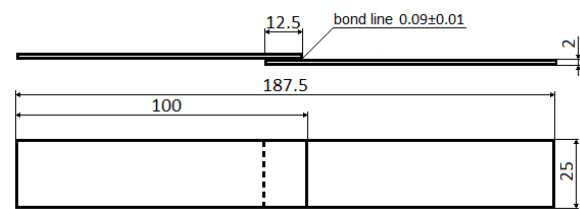


Fig. 1. Simplified scheme of an adhesive joint

The samples were subjected to a single-stage cold curing process for 72 hours (3 days) at a temperature of $22 \pm 1^\circ\text{C}$.

2.2. Pneumatic shot peening

Half of the adhesive joints were subjected to the pneumatic shot peening process to increase their load capacity. The pneumatic shot peening time was 120 s, the ball diameter was 1.0 mm, and the compressed air pressure was 0.5 MPa. Pneumatic shot peening was applied only to the surface of the joint overlap. The remaining part of the sample was covered. Both sides of the joint overlap were treated. The scheme of the adhesive joint prepared for pneumatic shot peening is shown in Fig. 2.

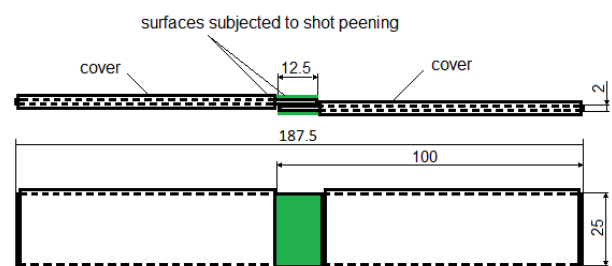


Fig. 2. Scheme of an adhesive joint prepared for pneumatic shot peening

2.3. Aging

The adhesive joints subjected to and not subjected to shot peening were aged in natural conditions. The aim of ageing was to determine the effect of long-term exposure to atmospheric conditions (daily and annual fluctuations in temperature and air humidity) on the load capacity of the adhesive joints subjected and not subjected to shot peening. The analyzes were carried out for 5 aging variants, which differed in length and months in which they were carried out (Table 2).

The samples were aged in a sunny location at ground level. Ageing conditions, including air temperature and relative humidity over 24 months (from 12/07/2021 to 12/07/2023), are shown in Figure 3. The measurements were taken in southern Poland.

Table 2. Aging variants

Start date	End date	Length	Marking (not shot peened)	Marking (shot peened)
12/07/2021	12/01/2022	6 months	6NP	6P
12/01/2022	12/07/2022	6 months	6NPW	6PW
12/07/2021	12/03/2022	9 months	9NP	9P
12/07/2021	12/07/2022	12 months	12NP	12P
12/07/2021	12/07/2023	24 months	24NP	24P
Not subject to aging			N	P

2.4. Static tensile test

The load capacity of the adhesive joints was determined using a static tensile test. The tests were carried out according to the methodology described in the PN-EN 1465:2009 standard using a ZWICK/ROELL Z100 test machine (Zwick/Roell, Ulm, Germany). In order to reduce the influence of tearing on the test results, the machine jaws were moved relative to each other. The force at which the adhesive joint was broken was considered as its load capacity and designated as P_t .

3. Results and discussion

The experimentally determined load capacity values of the adhesive joints are presented in Table 3.

Table 3. Load capacity of adhesive joints

Variant			Load capacity, N							Average load capacity, N	Standard deviation, N
			P_{t1}	P_{t2}	P_{t3}	P_{t4}	P_{t5}	P_{t6}	P_{t7}		
Not subjected to shot peening	Not aging	N	8163	6164	6110	6535	7959	8396	7938	7324	932
	Subjected to aging	6NP	8874	8489	10328	7128	7821	8024	8634	8471	931
		6NPW	5324	7362	5059	6610	7036	5854	4051	5899	1095
		9NP	9916	6889	5071	7272	8652	6710	7458	7424	1418
		12NP	9938	8315	10873	10437	10584	10613	9805	10081	802
	24NP	7160	7876	7374	7614	7215	7559	7411	7458	229	
Subjected to shot peening	Not aging	P	9553	9024	9273	9653	9237	10507	10815	9723	629
	Subjected to aging	6P	4573	5116	3889	4072	4284	4826	4978	4534	433
		6PW	4062	3716	5299	5515	4869	4474	4385	4617	601
		9P	7668	5030	4574	4953	5998	4653	2980	5122	1331
		12P	4150	4058	4868	4591	3955	4953	3017	4227	614
	24P	4490	3048	3863	3819	3514	3714	3583	3722	403	

Figure 4 shows the average values of the load capacity and the standard deviation for 12 sample variants. The average values were obtained based on 7 measurement samples.

Based on the results, it can be concluded that aging of adhesive joints not subjected to pneumatic shot

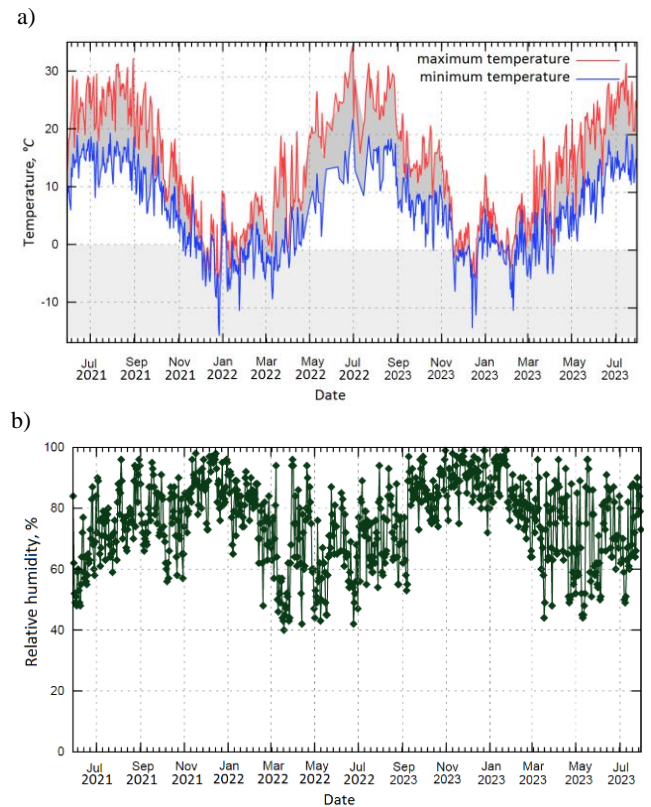


Fig. 3. Air temperature and humidity in the period July 2021 - July 2023 (24 months)

peening contributes to increasing their load capacity by 38% (maximum). The increase in the load capacity of joints due to aging may be the effect of additional crosslinking of the adhesive structure under the influence of elevated temperature in the summer season. Polymer materials (including adhesives)

exposed to long-term high temperature undergo thermal degradation which consists in the breakdown of macromolecules into smaller fragments. As a result of degradation, the crosslinking of the adhesive structure increases, which in the initial phase of the process can contribute to increasing the load capacity of the joints. However, in a later phase, the adhesive structure may undergo excessive crosslinking, the molecular weight may decrease, and, as a result, the strength properties of the adhesive joint may deteriorate (Rojek, 2011, Szabelski et al., 2019). According to the research results, the highest load is achieved by joints aged 12 months. After 24 months, the load capacity is already lower. The reason for the lower load capacity of the connections aged 24 months may be excessive crosslinking of the adhesive structure. Aging for six months from July increased the load capacity of the adhesive joints. In turn, the six-month ageing starting in January decreased the load capacity of the connections. Low winter temperatures did not allow additional crosslinking of the adhesive structure, but could have contributed to damage of the adhesive and cohesive bonds.

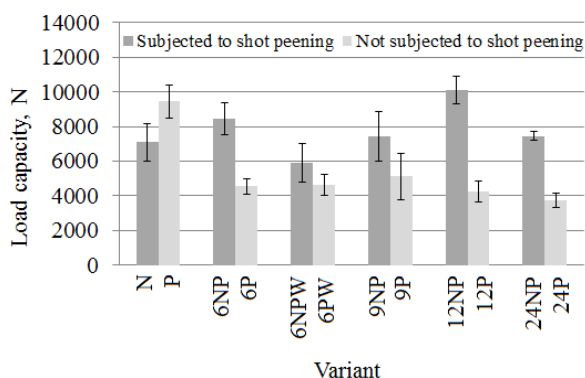


Fig. 4. Average load capacity of adhesive joints with standard deviation

Before aging, the load capacity of the joints subjected to shot peening is significantly higher than the load capacity of the joints that were not subjected to this treatment. As a result of shot peening, the elements are deformed, the edge of the overlap is pressed against the adherend, and compressive stresses are established in the bond line. Therefore, the joint load capacity increases. However, aging of joints previously subjected to shot peening reduces their load capacity by 62%. The reduction in the load capacity of the joints after aging may be caused by adhesive and cohesive bonds damage resulting from too intensive shot peening, degradation of the adhesive structure and the accumulation of stresses introduced during shot peening and resulting from temperature changes during aging. In contrast to connections not subjected to shot peening, six-month aging of shot-peened

connections had a similar effect, regardless of when it was started (in summer or winter).

The failure patterns of adhesive joints were analyzed according to the PN-EN ISO 10365:2022-07 standard. The aim of the failure patterns analysis was to check whether the use of the shot peening process had an impact on the nature of the destruction of adhesive joints. The classification of the failure patterns was made on the basis of visual inspection. Figures 5-6 show the view of the deteriorated adhesive joints subjected and not subjected to shot peening and aged for 6 months from July to January.



Fig. 5. Adhesive joints not subjected to shot peening and aged for 6 months from July to January

Based on Figures 5-6, it can be concluded that the nature of the destruction of the joints subjected to and not subjected to shot peening differs significantly. In both cases, however, adhesive and cohesive failure mechanisms can be observed.

In the case of joints not subjected to shot peening (Fig. 5), an adhesive failure (AF) is visible at the ends, while an adhesive-cohesive failure (AF and CF) occurs in the middle of the bond line. The failure patterns change with the distance from the edge of the

bond line. Adhesive failure, visible at the ends of the bond line, may indicate that the maximum stresses in joints subjected to tension are located at the ends of the bond line.

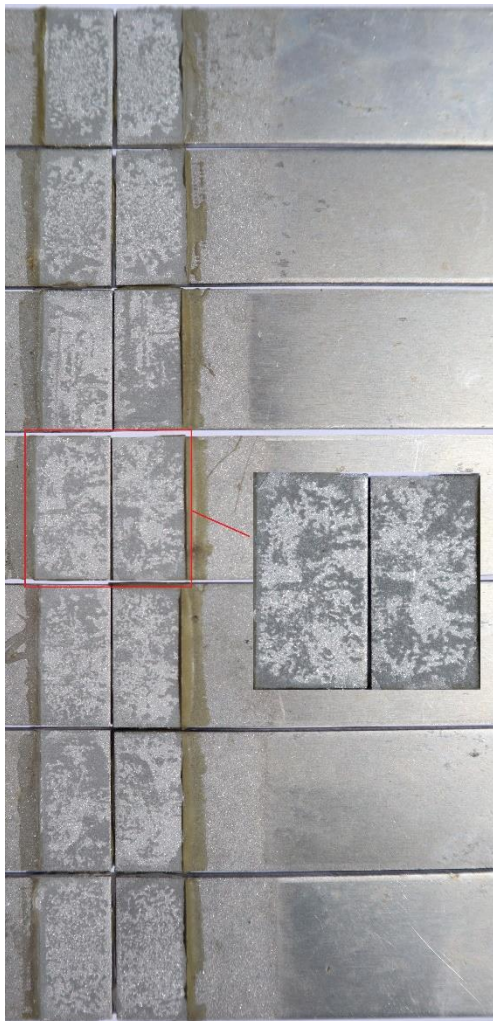


Fig. 6. Adhesive joints subjected to shot peening and aged for 6 months from July to January

In the case of joints subjected to shot peening, an adhesive-cohesive failure (AF and CF) can be observed along the entire length of the bond line. There is no visible adhesive failure zone at the ends of the bond line. Therefore, it can be assumed that, in the case of joints subjected to shot peening, the stress distribution in the bond line of the joint subjected to tension was more uniform than in the case of joints not subjected to shot peening. On the basis of the analysis of failure patterns, it can also be concluded that shot peening of the joint overlap could have affected the strength of adhesive and cohesive bonds.

The load capacity values obtained experimentally were subjected to statistical analyzes. Hypotheses in the statistical analyzes were tested for a significance level of $\alpha = 0.05$. This level of significance is most often used in research in the field of mechanical

engineering. The analyzes assumed the normality of the data distribution and the homogeneity of variance. The analyzes were performed using the Minitab and MS Excel programs.

In the first step, an analysis of variance (ANOVA) was performed. The purpose of this analysis was to determine whether the differences between the mean load capacity values of the comparative groups were the result of chance or a deliberate change in the level of the input factor, which is the length of aging. The analysis was performed separately for joints subjected to and not subjected to shot peening. The results of the tests obtained for joints aged 6 months from January (variants 6NPW and 6PW) were not subjected to statistical analyzes, because these joints were characterized by a lower load capacity than joints aged 6 months from July. The results of the analyzes are presented in Tables 4-5.

Table 4. Results of analysis of variance (ANOVA) - adhesive joints not subjected to shot peening

Source	Degrees of freedom	Sum of squares	Mean sum of squares	F statistic	Probability (<i>PvI</i>)
Regression	3	32634905	10878302	10.44	<0.001
Residual Error	24	25010438	1042102		
Total	27	57645343			

Table 5. Results of analysis of variance (ANOVA) - adhesive joints subjected to shot peening

Source	Degrees of freedom	Sum of squares	Mean sum of squares	F statistic	Probability (<i>PvI</i>)
Regression	3	7235076	2411692	3.31	0.037
Residual Error	24	17488549	728690		
Total	27	24723625			

Based on the results of the analysis of variance (ANOVA), it can be stated that for the assumed range of input factor variability, the aging time has a significant effect on the load capacity of adhesive joints not subjected to pneumatic shot peening (Table 4) and subjected to pneumatic shot peening (Table 5). This is confirmed by the probability PvI values, which in both cases are less than 0.05.

The conclusions of the analysis of variance are confirmed by the box plots presented in Figure 7b.

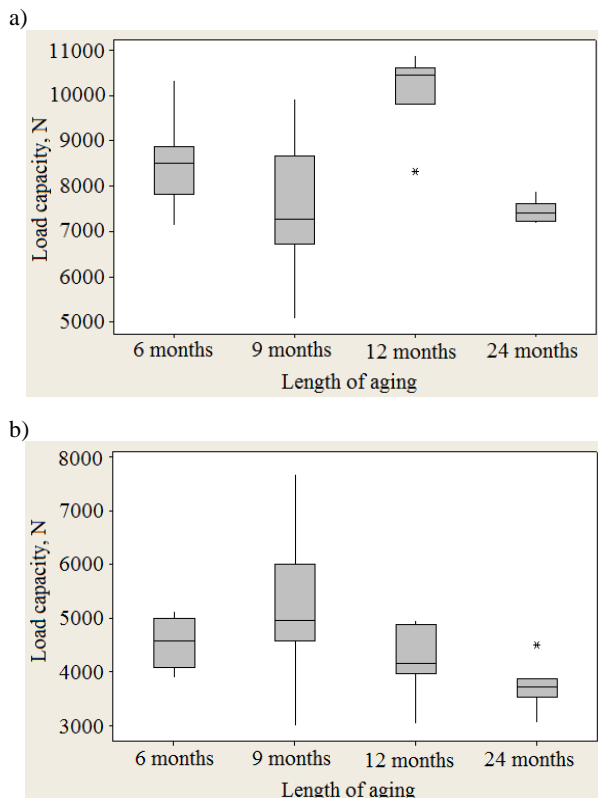


Fig. 7. Box plots: a) adhesive joints not subjected to shot peening, b) subjected to shot peening

Based on the box plots, it can be concluded that the smallest interquartile range is observed for connections aged for 24 months, which indicates the smallest variation in the load capacity of the connections belonging to this variant. In this case, ageing leads to stabilization of the strength properties of the connections. The greatest variation in the load capacity values is observed for the connections aged 9 months. The symbol (*) in the figures indicates the upper extreme value (value greater than the sum of the third quartile value and the interquartile range multiplied by 3) and the lower extreme value (value less than the difference of the third quartile value and the interquartile range multiplied by 3).

Analysis of variance (ANOVA) allowed to state that at least one of the analyzed groups differed significantly from another group. To check which

groups differed statistically significantly, the Student's t test was performed. Student's t test was used to compare the mean values of load capacity between two groups. The results of the test are presented in Tables 6-7.

Table 6. Student's t test results for joints not subjected to shot peening

$Pv2$ [%]	N	6NP	9NP	12NP	24NP
N	-				
6NP	2.706	-			
9NP	44.375	8.018	-		
12NP	0.007	0.385	0.141	-	
24NP	37.055	1.866	47.750	0.006	-

Table 7. Student's t test results for joints subjected to shot peening

$Pv2$ [%]	P	6P	9P	12P	24P
P	-				
6P	<0.001	-			
9P	0.002	16.812	-		
12P	<0.001	16.991	8.559	-	
24P	<0.001	0.278	2.112	5.986	-

In the case of connections not subjected to shot peening (Table 6), a statistically significant difference was obtained in the average load capacity for connections aged for 12 months. Statistically significant differences in the average load capacity also occur between connections that were not aged (N) and aged for 6 months (6N) and between connections that were not aged (N) and aged for 24 months (24N). In the case of connections subjected to shot peening, the average load capacity of connections that were aged and connections that were not aged, connections that were aged for 6 months (6P) and 24 months (24P), as well as, connections that were aged 9 months (9P) and 24 months (24P) are statistically significantly different. The results indicate that ageing can significantly increase the load capacity of connections that were not previously strengthened by shot peening. The best effect is observed in the case of ageing for 6 and 12 months. Aging of shot-peened joints significantly reduces their load capacity (irrespective of the ageing length).

In order to check the strength of the linear relationship between the input variable (ageing length) and the output variable (load capacity of adhesive joints), the values of the Pearson linear correlation coefficient $r_{y/x}$ were calculated. The linear correlation coefficient can range from -1 to 1. The closer the coefficient value is to 0, the weaker the linear

relationship between the variables. As part of the statistical analyzes, linear regression equations were also determined. The equations describe the effect of

the length of ageing on the load capacity of adhesive joints. The results of the regression and correlation analyzes are presented in Table 8.

Table 8. Results of regression and correlation analysis

Output variable	Input variable	Regression equation	$Pv3^2$	Coefficient of determination	Correlation coefficient $r_{y/x}$
Load capacity (joints not subjected to shot peening) P_{tNP}	Length of aging T_s	$P_{tNP} = 8951 - 46.4T_s$	0.258	1.23%	-0.22
Load capacity (joints subjected to shot peening) P_{tP}	Length of aging T_s	$P_{tP} = 5162 - 59.7T_s$	0.021	18.72%	-0.43

² $Pv3$ - probability level for an independent variable in regression analysis

Based on the regression equations and the Pearson linear coefficients, it can be concluded that the load capacity of the joints decreases with increasing aging length. However, in the case of regression analysis for joints not subjected to shot peening, the probability value $Pv3$ is greater than 0.05. Therefore, the regression equation cannot be used to describe the relationship between the load capacity of the joints and the length of aging. The values of the coefficient of determination indicate that the changes in load capacity are the result of the change in aging length by approximately 2% for joints not subjected to shot peening and by approximately 19% for shot peened joints.

4. Conclusions

Based on the analyzes, it can be stated that for the assumed range of input factor variability, the ageing of the joints not subjected to shot peening contributed to an increase in their load capacity by 38%. The greatest increase in load capacity was observed in the case of ageing for 12 months. Extending the ageing time to 24 months resulted in a slight decrease in load capacity. However, samples aged for 24 months are characterized by the smallest dispersion of load capacity values, which may indicate stabilization of strength properties as a result of ageing. The six-month ageing that began in July increased the load capacity of the joints. In turn, six-month ageing started in January decreased the load capacity of connections.

Ageing of joints subjected to shot peening reduced their load capacity by 62%. The lowest load capacity was observed for joints aged 24 months.

Statistical analyzes have shown that the length of ageing can have a significant effect on the load capacity of adhesive joints.

It has been shown that there is a weak linear negative correlation between the extension of the ageing time and the load capacity of the adhesive joints.

In summary, the results prove that aging of adhesive joints is justified, unless they were previously subjected to strengthening in the pneumatic shot peening process. It is also worth noting that aging has a positive effect on the strength properties of joints when it is carried out in the summer months (not winter).

Further research could be directed towards determining the effect of ageing on the load capacity of joints shot peened with lower intensity. It is also justified to investigate the effect of thermal shocks on the load capacity of joints subjected to and not subjected to shot peening.

References

- Bahrami, B., Ayatollahi, M.R., Beigrezaee, M.J., da Silva, L.F.M. (2019). Strength improvement in single lap adhesive joints by notching the adherends. *International Journal of Adhesion and Adhesives*, 95, 102401.
- Belingardi, G., Goglio, L., Tarditi, A. (2002). Investigating the effect of spew and chamfer size on the stresses in metal/plastics adhesive joints. *International Journal of Adhesion and Adhesives*, 22 (4), 273-282.
- Bowditch, M.R. (1996). The durability of adhesive joints in the presence of water. *International Journal of Adhesion and Adhesives*, 16 (2), 73-79.
- Çalık, A. (2016). Effect of adherend shape on stress concentration reduction of adhesively bonded single lap joint. *Engineering Review*, 36(1), 29-34.
- Dobrzański, L.A. (2010). *Leksykon Materialoznawstwa. Praktyczne zestawienie norm polskich, zagranicznych i międzynarodowych. Cz. 4, rozdział 1: Metale nieżelazne i ich stopy*. Wydawnictwo Verlag Dashofer.
- Durmuş, M., Akpınar, S. (2019). The Experimental and Numerical Analysis of the Adhesively Bonded Three-step-Lap Joints with Different Step Lengths. *Theoretical and Applied Fracture Mechanics*, 105, 102427.
- Godzimirski, J., Jagiełło, A. (2018). Effect of surface treatment cold-work hardening after adhesive curing on strength of adhesive lap joints. *Technologia i Automatyizacja Montażu*, 4, 43-49.

- Henkel Polska Sp. z o.o. (24.06.2024). Technical Data Sheet Loctite EA 3430. chrome-extension://efaidnbmnnnibpcajpcglclefindmkaj/https://datasheets.tdx.henkel.com/LOCTITE-EA-3430-en_GL.pdf
- Hirulkar, N.S., Jaiswal, P.R., Reis, P.N.B., Ferreira, J.A.M. (2020). Effect of hygrothermal aging and cyclic thermal shocks on the mechanical performance of single-lap adhesive joints. *International Journal of Adhesion and Adhesives*, 99, 102584.
- Morcos, M., Challita, G., Legrand, V., Khalil, K., Casari P. (2022). Impact strength of thermally aged double lap adhesively bonded joints. *International Journal of Adhesion and Adhesives*, 112, 103029.
- Ozga, E. (2023). *Wpływ pneumokulkowania na nośność połączeń klejowych ze stopu aluminium EN AW-2024-T3*. [Rozprawa doktorska]. Politechnika Rzeszowska im. Ignacego Łukasiewicza.
- Polski Komitet Normalizacyjny. (2009). *Kleje – Oznaczenie wytrzymałości na ścinanie przy rozciąganiu połączeń na zakładkę* (PN-EN 1465:2009).
- Polski Komitet Normalizacyjny. (2018). *Aluminium i stopy aluminium – Blachy, taśmy i płyty – Część 2: Własności mechaniczne* (PN-EN 485-2+A1:2018-12).
- Polski Komitet Normalizacyjny. 2022. *Kleje – Oznaczenie głównych wzorców zniszczenia połączeń klejowych* (PN-EN ISO 10365:2022-07).
- Rojek, M. (2011). Metodologia badań diagnostycznych warstwowych materiałów kompozytowych o osnowie polimerowej. *Open Access Library*, 2.
- Szabelski, J., Domińczuk, J., Kuczmaszewski, J. (2019). *Wpływ ciepła na właściwości połączeń klejowych*. Wydawnictwo Politechniki Lubelskiej.
- Zhao, X., Adams, R. D., da Silva, L. F. M. (2011). Single Lap Joints with Rounded Adherend Corners: Stress and Strain Analysis. *Journal of Adhesion Science and Technology*, 25(8), 819-836.
- Zielecki, W. (2008). *Determinants determining the strength properties of adhesive joint*. [Rozprawa habilitacyjna]. Uniwersytet Techniczny w Koszycach.
- Zielecki, W., Bielenda, P., Ozga, E. (2021). The influence of thermal shock on the load capacity of cylindrical adhesive joints made of EN AC-ALSI7-Mg0.3 aluminum alloy and glass-epoxy composite EP405-GE. *Technologia i Automatykacja Montażu*, 4, 34-42.
- Zielecki, W., Guźla, E., Bielenda, P. (2021). The influence of natural seasoning on the load capacity of cylindrical adhesive joints. *Technologia i Automatykacja Montażu*, 3, 15-24.

ANALYSIS OF THE POSSIBILITIES OF IMPLEMENTING ALTERNATIVE METHODS OF JOINING SEMIFINISHED PRODUCTS IN THE PRODUCTION PROCESS OF STEEL RIMS

ANALIZA MOŻLIWOŚCI WDROŻENIA ALTERNATYWNYCH METOD ŁĄCZENIA PÓŁWYROBÓW W PROCESIE PRODUKCJI FELG STALOWYCH

Izabela MITURSKA-BARAŃSKA^{1,*} , Michał BORNUS², Rafał SZADURA²

¹ Lublin University of Technology, Faculty of Mechanical Engineering, Department of Computerization and Production Robotization, Nadbystrzycka 36, 20-618 Lublin, Poland

² MW Lublin Sp. z o.o., Mełgiewska 7/9, 20-209 Lublin, Poland

* Corresponding author: i.miturska@pollub.pl

Abstract

Assembly technology plays a crucial role in the manufacturing process, influencing the efficiency, quality, cost and lead time of production. Assembly technology in the manufacturing process encompasses all techniques and methods used to join components into a finished product. Depending on the industry and specific requirements, assembly technologies can include a variety of techniques, from traditional mechanical joints to advanced bonding, welding or soldering methods. The paper analysed the feasibility of implementing alternative methods of joining blanks in the steel wheel manufacturing process. Testing was carried out to replace the wheel rim flash welding process with laser welding. The effectiveness of laser welding was evaluated by testing prepared butt jointed sheet samples. Tests were carried out on two types of structural steel: S355MC and DD11, which were subjected to flash welding and laser welding. The specimens were subjected to strength and macrographic tests to analyse their structure and mechanical properties. The results showed that laser welding for DD11 steel leads to an increase in tensile strength, while for S355MC steel this strength is reduced. Statistical analysis showed no significant differences between the assembly methods used and the steel types. Macrographic tests confirmed the presence of oxides and other characteristics of the assembly methods used. The results suggest that the choice of the appropriate joining method can have a significant impact on the quality and durability of the final product, which is crucial in the context of steel wheel production.

Keywords: assembly, flash welding, laser welding, strength

Streszczenie

Technologia montażu odgrywa kluczową rolę w procesie produkcyjnym, wpływając na efektywność, jakość, koszty oraz czas realizacji produkcji. Technologia montażu w procesie produkcyjnym obejmuje wszystkie techniki i metody używane do łączenia komponentów w gotowy produkt. W zależności od branży i specyficznych wymagań, technologie montażu mogą obejmować różnorodne techniki, od tradycyjnych połączeń mechanicznych po zaawansowane metody klejenia, spawania czy lutowania. W pracy przeanalizowano możliwości wdrożenia alternatywnych metod łączenia półwyrobów w procesie produkcji felg stalowych. Przeprowadzono próby zastąpienia procesu zgrzewania iskrowego obręczy koła spawaniem laserowym. Skuteczność spawania laserowego oceniano badając przygotowane próbki blach łączonych doczołowo. Badania przeprowadzono na dwóch rodzajach stali konstrukcyjnej: S355MC i DD11, które zostały poddane zgrzewaniu iskrowemu oraz spawaniu laserowemu. Próbki poddano testom wytrzymałościowym oraz makrograficznym w celu oceny ich struktury i właściwości mechanicznych. Wyniki badań wykazały, że spawanie laserowe w przypadku stali DD11 prowadzi do wzrostu wytrzymałości na rozciąganie, podczas gdy w przypadku stali S355MC wytrzymałość ta ulega obniżeniu. Analiza statystyczna nie wykazała istotnych różnic między zastosowanymi metodami montażu a rodzajami stali. Badania makrograficzne potwierdziły obecność tlenków oraz inne cechy charakterystyczne dla zastosowanych metod montażu.

Wyniki sugerują, że wybór odpowiedniej metody łączenia może mieć istotny wpływ na jakość i trwałość końcowego produktu, co jest kluczowe w kontekście produkcji felg stalowych.

Słowa kluczowe: montaż, zgrzewanie iskrowe, spawanie laserowe, wytrzymałość

1. Introduction

Assembly technology plays a fundamental role in many industries, including the automotive industry, affecting almost every aspect of vehicle production (Uchihara, 2011). First and foremost, effective assembly technology is crucial to ensure high quality and precision in production, which translates into safety, reliability and durability of finished vehicles. Advanced assembly methods such as automation, robotics and techniques such as welding, resistance welding and bonding enable the creation of components with high strength and accuracy (K Srivastava & Sharma, 2017).

The implementation of high-tech assembly technologies significantly improves manufacturing efficiency, allowing for rapid and automated assembly of parts, which reduces production time and manufacturing costs (Cohen, Naseraldin, Chaudhuri, & Pilati, 2019). As a result, automotive companies can produce vehicles on a larger scale, meeting growing market demand while maintaining competitive prices.

One of the steps in the vehicle manufacturing process is the steel wheel production process, where assembly technology plays a crucial role, influencing every stage of the product creation. First and foremost, proper assembly methods ensure that the various parts of the rim, such as the rim and disc, are precisely and permanently joined together, which is essential to ensure the safety and reliability of the finished product. Advanced techniques, such as laser welding or flash welding, make it possible to create high-strength joints while minimising the weight of the rim, which is important for vehicle performance (Fysikopoulos, Pastras, Stavridis, Stavropoulos, & Chryssoulouris, 2016).

The implementation of high-tech assembly technologies also affects the efficiency of the manufacturing process. The automation and robotisation of assembly processes allows an increase in production speed, while reducing the risk of defects and lowering manufacturing costs (Perka, John, Kuruveri, & Menezes, 2022; Xu, Shi, Cui, & Liang, 2023). As a result, higher production efficiencies can be achieved, which has a direct impact on competitiveness in the automotive industry.

Assembly technology also influences production flexibility, enabling rapid adaptation to changing industry requirements, such as the introduction of new rim models. In addition, choosing the right assembly

methods is environmentally relevant, as it can lead to a reduction in energy and material consumption, which promotes sustainable production. As a result, assembly technology is a crucial element in the production process of steel rims, having a direct impact on the quality, efficiency and innovation of the final product (I Miturska & Rudawska, 2021; I Miturska, Rudawska, Pawlak, Stančėková, & Chyra, 2017).

Another important aspect is the sustainability impact of assembly technology. Choosing energy-efficient and less resource-intensive assembly methods contributes to reducing the carbon footprint of the production process, which is increasingly important in the context of global environmental requirements (K Srivastava & Sharma, 2017; Szala & Lukasik, 2018).

The aim of this study was to carry out a specific analysis of the possibility of implementing alternative methods of joining blanks in the production process of steel wheels. This analysis was made possible by assessing the efficiency and strength of the joints made using laser welding, compared to the traditional method so far used in the process under study, which is flash welding. Two types of structural steel were used in this study: S355MC and DD11. From these materials, specimens were prepared by butt welding and laser welding. The joints were tested for strength and structural properties.

1.1. Flash butt welding

Flash welding is an assembly method that plays a fundamental role in the process of joining metals, especially in the automotive, construction and appliance industries. The process involves welding the ends of two metal parts that are pressed together and heated simultaneously, leading to melting and re-solidification (Kimchi & Phillips, 2023). During flash butt welding, it is important that the quality and characteristics of the weld are adequate, as these determine the strength and durability of the joint. The weld is often homogeneous with the base materials to ensure good electrical conductivity and favourable mechanical properties. Flash butt welding is used in the manufacture of cables, pipes, as well as in the construction of automobiles and various appliances (Al-Mukhtar, 2016).

There are several steps in the electrical flash welding process, which is the most commonly used method. Initially, the workpieces are pressed against

each other and then an electric current is switched on, leading to the release of heat at the contact surface. As the temperature rises, the metal plasticises and the pressing force causes deformation. When the current is switched off, the weld remains under pressure, allowing the metal to solidify (Biradar & Dabade, 2020).

The main methods used in the electrical spark welding process are alternating current (AC) and direct current (DC) welding (Balaraju, Sankara Narayanan, & Seshadri, 2003; Hajializadeh & Mashhadi, 2015). These methods differ in both equipment design and process characteristics.

AC resistance welding involves the use of alternating current, which means that the supply voltage changes direction at regular intervals. With AC resistance welding machines, the resistance welding process relies on transformers that convert the mains voltage to the appropriate values for the resistance welding process.

On the other hand, DC flash welding uses direct current, which allows for a more stable and controlled flash welding process. DC-powered devices can be designed as three-phase spark welding machines or average frequency inverters (MF/DC). DC flash welders are characterised by a higher power rating and better control of the spark welding parameters, resulting in higher joint quality. With DC flash welding, the current is rectified, resulting in more homogeneous and stronger welds.

In the process of manufacturing steel wheels, both of the methods described are applicable.

1.2. Laser welding

Laser sheet metal welding is a modern material joining technique that uses a concentrated laser beam as a heat source to fuse the edges of the parts to be joined. This method is characterised by high precision, speed and minimal impact on surrounding materials, making it an attractive alternative to traditional flash welding techniques (Mei et al., 2015; Mei, Yi, Yan, Liu, & Chen, 2012).

In laser welding, there are two main modes: conduction welding and deep-fusion welding. In conduction welding, the laser beam heats the surface of the material to its melting point, leading to the formation of a weld pool (Hong & Shin, 2017). This technique is particularly effective for thin-film materials where the aesthetics of the weld are important. Deep-fusion welding, on the other hand, involves heating the material to the point of evaporation, resulting in deeper and narrower welds, ideal for joining thick plates (Manoharan, Bashir, & Zaifuddin, 2020; Rossini, Spena, Cortese, Matteis, & Firrao, 2015).

One of the main advantages of laser welding is the small heat affected zone, which minimises the risk of material distortion and subsequent processing requirements. The high precision and repeatability of the process make laser welding widely used in a variety of industries.

These techniques also make it possible to join materials with different properties, such as steel and aluminium, which is important in the context of modern construction where material diversity is common. Laser welding can be used in both continuous and pulsed modes, allowing the process to be adapted to specific production requirements (Fernandes, Oliveira, & Pereira, 2017).

The development of laser technology and the automation of welding processes in recent years have contributed to increased efficiency and lower production costs, making laser welding increasingly popular in industry. As technology advances, this method can be expected to develop further, opening up new possibilities for joining materials (Manoharan et al., 2020).

2. Experimental studies

2.1. Materials

The materials used in the study were sheets of two types of structural steel: S355MC and DD11, which are used in the manufacturing process of steel wheels.

S355MC steel is a type of structural steel that is characterised by increased strength, $R_m = 430\text{-}550$ MPa, and good ductility with a minimum yield strength of 355 MPa (https://www.steelnumber.com/en/steel_composition_eu.php?name_id=206, 2024). S355MC steel is particularly valued in civil engineering, where it is used for structures subjected to dynamic and fluctuating loads. The chemical composition of S355MC steel is shown in Table 1.

Table 1. Chemical composition % of steel S355MC (https://www.steelnumber.com/en/steel_composition_eu.php?name_id=206, 2024)

Component	Amount
C	max 0.120
Si	max 0.500
Mn	max 1.500
P	max 0.025
S	max 0.020
V	max 0.200
Nb	max 0.090
Ti	max 0.150
Al	max 0.015
The sum of Nb, V and Ti shall be max 0.22 %	

It is worth pointing out that S355MC steel is used in a variety of industries, including the automotive industry, where it is used to manufacture components subjected to varying loads. Its properties make it suitable for applications requiring high strength and durability.

The second material used in the study was DD11 steel. DD11 steel has excellent ductility, with a minimum yield strength of 360 MPa and a strength of $R_m = 440$ MPa (https://www.steelnumber.com/en/steel_composition_eu.php?name_id=218, 2024). The chemical composition of DD11 steel is shown in Table 2.

Table 2. Chemical composition % of steel DD11 (https://www.steelnumber.com/en/steel_composition_eu.php?name_id=218, 2024)

Component	Amount
C	max 0.120
Mn	max 0.600
P	max 0.045
S	max 0.045

The properties of DD11 steel make it suitable for a variety of applications, such as load-bearing structures and transport components. Although it is not galvanised, its surface is adequately protected against corrosion, which increases its durability in industrial applications. The steel is also abrasion resistant, which is an important advantage in applications where the material is exposed to intensive use and mechanical stresses.

2.2. Specimens

Specimens prepared from the materials described were used for testing. Strips of sheet metal with the dimensions shown in Figures 1 and 2 were joined together, and the specimens to be tested were then cut out, with a width of 25 mm.

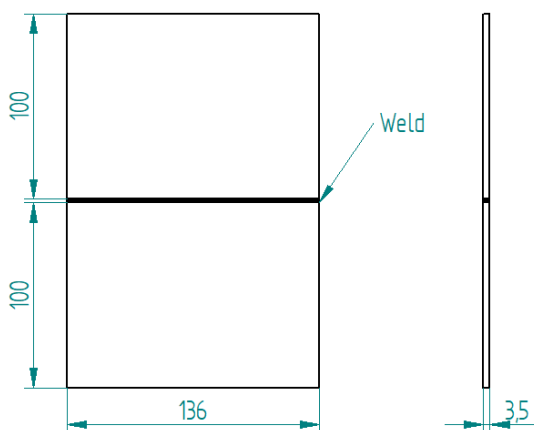


Fig. 1. Dimensions and geometry of S355MC steel specimens

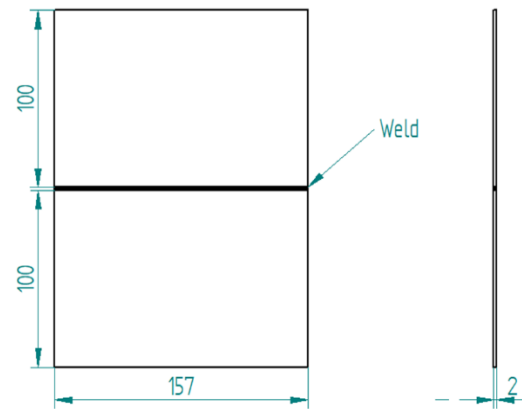


Fig. 2. Dimensions and geometry of DD11 steel specimens

For comparison purposes, the native material was also tested. For this purpose, specimens of 100 mm x 25 mm were cut from sheets of each material. The thickness of the specimens depended on the type of material, as shown in Figures 1 and 2. 10 specimens were prepared for each type of joint and each material.

2.3. Specimens preparation

The specimens to be tested were prepared using two assembly methods: electrical flash welding and laser welding.

2.3.1. Electric flash welding

The welding process was carried out in accordance with the guidelines that apply to the production process for steel wheels. The material was not specially prepared before the process. Some of the data relating to the welding process is confidential and therefore not all data can be made public. The butt-welding process was carried out using a DC welding machine with a 630 kVA transformer. The electrodes used in the process are made of CNCS copper and are 280 mm long. After the butt-welding process, the weld was trimmed and rolled in the specimens to be tested for strength, in order to remove the hump created during the weld forming process, according to the guidelines of the actual process.

2.3.2. Laser welding

The alternative assembly method proposed for butt flash welding the sheets was laser welding. In order to replicate the production conditions as possible, the materials were not subjected to any special treatment before the welding process. Laser welding was realised using a Fanuci 4.0 Pro GenX handheld welding laser with a fibre source power of 3kW. The components of the laser welding station are shown in Figure 3.



Fig. 3. Construction of a laser welding station

The working tool in the laser welding station, and at the same time the most essential one, is the laser head. Its construction is shown in Figure 4.

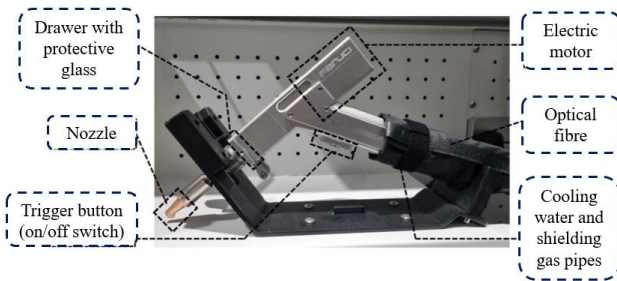


Fig. 4. Construction of a GenX laser head

Taking into account the properties of the materials to be joined and their dimensions, in particular the thickness, appropriate parameters were selected for the laser welding process. The welding parameters used are summarised in Table 3.

Table 3. Process parameters for laser welding

Parameter	S355MC	DD11
Welding wire	Ø1.6 mm Esab OK Autrod 12.64	Ø1.6 mm Esab OK Autrod 12.64
Shielding gas	100% argon Compressed argon 2.2	100% argon Compressed argon 2.2
Scanning width	3.0 mm	3.0 mm
Power	1 450 W	1 500 W
Wire feed speed	400 mm/min	800 mm/min
Scanning speed	300 mm/s	300 mm/s
Frequency	5 000 Hz	5 000 Hz

Using the above parameters, the sheets were butt jointed.

3. Research results and discussion

The specimens were subjected to strength tests and macrographic tests to assess their structure. The results obtained are shown below.

3.1. Strength test results

Strength tests were carried out using a Zwick Roell Z150 strength testing machine in accordance with PN-EN 10002-1:2004 test standard (*PN-EN 10002-1:2004 - Metallic materials - Tensile testing - Part 1: Method of test at ambient temperature*, 2004). The results are shown in Figures 5 and 6.

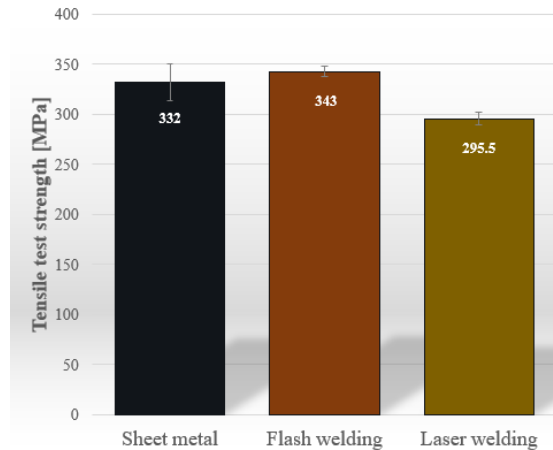


Fig. 5. Test results of tensile test strength of S355MC

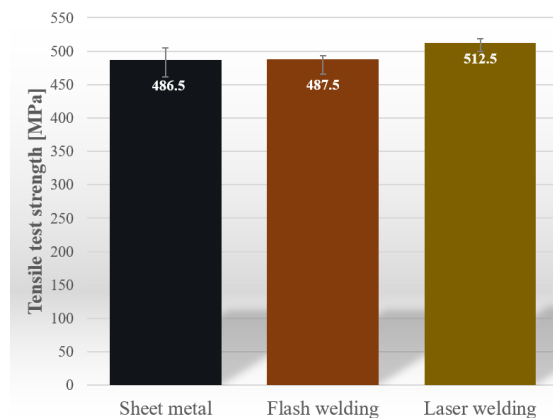


Fig. 6. Test results of tensile test strength of DD11

The obtained test results show that for the specimens made of S355MC sheet the average tensile strength for the raw sheet is 332 MPa, which is the basis for comparison with the samples after welding. The average tensile strength after flash welding increases slightly to 343 MPa. This slight increase suggests that flash welding can lead to favourable changes in the microstructure of S355MC steel, which can strengthen the material. The low variability of the results indicates that flash welding is a reproducible process that does not result in large differences in tensile strength between samples. With laser welding, the tensile strength decreases to 295.5 MPa, which is the lowest value compared to the other samples. The decrease in strength after laser welding may be due to defects, such as microcracks or changes in the crystal structure, which can weaken the material. This can

also be evidenced by the fact that only in these joints did the failure occur at the weld site. The standard deviation of all analysed groups of samples represents between 1.6 % and 5.5 % of the average strength, suggesting that the strength test results were stable and did not show much variability. This means that the material had a uniform structure and consistent mechanical properties.

For the specimens made from DD11 sheet, the average tensile strength value for the reference specimens is 486.5 MPa. For the flash-welded specimens, the strength increases minimally to 487.5 MPa, suggesting that this method does not have a significant effect on reducing the strength of the material. For the laser-welded specimens, the average tensile strength increases to 512.5 MPa, indicating an improvement in the material's mechanical properties compared to the baseline.

A statistical analysis of the results obtained was also carried out to verify whether the differences occurring between the various assembly methods and materials were significant. A significance level of $\alpha=0.05$ was adopted and a one-way ANOVA analysis was performed. However, the results obtained did not show any significant differences between the results analysed.

3.2. Macrographic results

The results of the macrographic tests are shown in the figures in Tables 7-10. The samples were polished to check for the presence of oxides on the surface and etched using the Bechet-Beaujet method to better examine the internal geometry of the weld.

Table 7. Macrographic test results - flash welding joints of S355MC steel







Section	Polishing only	Etching Bechet-Beaujet
Start		
Centre		
End		

Table 8. Macrographic test results - laser welding joints of S355MC steel











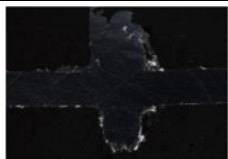
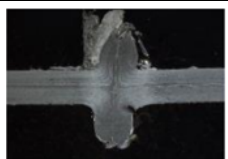
Section	Polishing only	Etching Bechet-Beaujet
Start		
Centre		
End		







Table 9. Macrographic test results - flash welding joints of DD11 steel

Section	Polishing only	Etching Bechet-Beaujet
Start		
Centre		
End		

The aim of the macrographic tests was, among other things, to check for the presence of oxides on the bonded surface. The presence of oxides can affect the quality of the weld and lead to defects that can weaken the strength of the joint. By analysing the cross-sections of the joints made of S355MC steel, it can be seen that in the case of flash-welded joints, oxides were not present on the surface. In the case of laser-welded joints, oxides were present on the surface of the weld. By analysing the cross-section of the etched specimens, it can be observed that, in the case of the

flash-welded specimens, characteristic structures are visible, indicating material flow at the joint. The laser-welded cross-sections presented structural defects. Inclusions, pores and impurities in the weld are visible. Such defects can affect mechanical properties, including fracture toughness and compressive and tensile strength.

Table 10. Macrographic test results - laser welding joints of DD11 steel

Section	Polishing only	Etching Bechet-Beaujet
Start		
Centre		
End		

By analysing the cross-sectional images of the joints made from DD11 steel, it can be seen that, as in the case of the specimens made from S355MC steel, oxides are present on the surface of the laser-welded joints. The flash-welded joints are characterised by a homogeneous structure. The microstructure in the weld cross-section of the laser-welded joints shows some inhomogeneities, such as the presence of inclusions, but in a smaller amount than in the laser-welded joints of S355MC sheet.

Laser welded joints have a large number of imperfections (visible pores), which can be caused by several factors.

Firstly, laser welding is a very precise technique, but in the case of materials with a complex microstructure, such as S355MC structural steel, defects such as micro-cracks or changes in the crystal structure can occur. Such defects can weaken the material, causing cracks or the formation of pores.

Secondly, Laser welding requires the precise selection of parameters such as laser power, welding speed or type of shielding gas. Improper settings can lead to excessive material evaporation or uneven melting, resulting in pores and other defects in the welds. In the study presented here, the parameters used

in the research were chosen experimentally, and perhaps an improvement in the parameters would have alleviated the problem in the weld structure.

Thirdly, the formation of oxides on the weld surface can occur during laser welding, as shown in the macrographic results. Oxides and other inclusions can lead to imperfections in the weld structure, weakening its strength and causing pores to form.

Fourthly, although there is a small heat affected zone in laser welding, which minimises material distortion, it can at the same time promote the formation of defects, particularly in areas of thicker material or where the filler material does not distribute uniformly.

In summary, it can be concluded that imperfections in the form of pores in laser welds are due to a combination of process-related factors such as micro-cracks, structural defects, the presence of oxides and difficulties in optimally setting the welding parameters.

4. Conclusion

Assembly technology is a fundamental aspect of steel wheel production, and plays an important role in ensuring the high quality and durability of the finished product. Tests carried out on samples of S355MC and DD11 steel, using two assembly methods - electrical flash welding and laser welding - allowed the efficiency and strength of the joints made using these techniques to be assessed.

The results of the strength tests showed that electrical flash welding provided more stable and repeatable joints, especially for S355MC steel, while laser welding, despite its higher precision, could lead to structural defects that weaken the material. In the case of DD11 steel, laser welding improved the mechanical properties compared to the baseline.

Macrographic tests revealed that oxides were present on the surface of laser-welded joints, which may affect the quality and strength of the joints, while flash-welded joints were characterised by a more homogeneous structure.

Based on the research carried out, the following conclusions can be formulated:

- Flash electric welding is a more efficient assembly method in terms of stability and repeatability of results, especially for S355MC steel, where it minimizes the risk of structural defects. This may be related to this method's lower propensity to cause structural defects in mild steels. The decrease in strength after laser welding may be due to increased brittleness or the formation of defects in the microstructure of the steel during welding.

- Laser welding can lead to microcracks and other defects that can reduce the strength of the joints, which was particularly evident in S355MC steel samples. However, in the case of DD11 steel, laser welding resulted in improved mechanical properties, suggesting that the method may be beneficial depending on the material used. This may be due to less heat input and a more homogeneous microcrystalline structure obtained during laser welding
- The comparison of the results shows that the mechanical properties and the choice of the appropriate joining technique can differ significantly depending on the type of steel, which should be taken into account in the design and production process. However, as the statistical analysis showed, in the analyzed cases the differences that occur are statistically insignificant.
- The cross-sectional analysis shows how various factors can affect the microstructure of the material at the junction. In the heat-affected zone, changes in the crystal structure can be expected, which can lead to the formation of phases such as martensite, bainite or pearlite, depending on the cooling process.
- The presence of oxides on the surface of laser-welded joints is a significant problem that can affect the durability and strength of the joints, which requires further research into optimizing laser welding parameters.
- Analysis of the etched samples shows that both flash-welds and laser-welds can contain structural inhomogeneities, such as changes in remelting geometry and the presence of micropores or inclusions. In the case of the DD11 material, which is a steel with good ductility but low strength, these defects can have a significant impact on the strength of the joints.
- The use of modern assembly technologies such as laser welding, despite some advantages, requires detailed analysis in the context of specific applications and material properties to guarantee optimal quality and durability of products.

In conclusion, the choice of an appropriate assembly method in the manufacturing process should always be made taking into account the specific properties of the materials used, application requirements, especially regarding the strength of the joints, cost effectiveness, as well as the impact on the environment and the sustainability of production. Therefore, in order to continue the discussed issue, further research will focus on optimizing laser welding

parameters, evaluating the durability of joints under operating conditions, and cost calculation taking into account the adaptation of the laser welding process in the actual production process of steel rims.

References

- Al-Mukhtar, A.M. (2016). Review of Resistance Spot Welding Sheets: Processes and Failure Mode. *Advanced Engineering Forum*, 17, 31–57. doi: 10.4028/www.scientific.net/AEF.17.31.
- Balaraju, J.N., Sankara Narayanan, T.S.N., Seshadri, S.K. (2003). Electroless Ni–P composite coatings. *Journal of Applied Electrochemistry*, 33(9), 807–816. doi: 10.1023/A:1025572410205.
- Biradar, A.K., Dabade, B.M. (2020). Optimization of resistance spot welding process parameters in dissimilar joint of MS and ASS 304 sheets. *Materials Today: Proceedings*, 26, 1284–1288. doi: 10.1016/j.matpr.2020.02.256.
- Cohen, Y., Naseraldin, H., Chaudhuri, A., Pilati, F. (2019). Assembly systems in Industry 4.0 era: A road map to understand Assembly 4.0. *The International Journal of Advanced Manufacturing Technology*, 105(9), 4037–4054. doi: 10.1007/s00170-019-04203-1.
- Fernandes, F.A.O., Oliveira, D.F., Pereira, A.B. (2017). Optimal parameters for laser welding of advanced high-strength steels used in the automotive industry. *Procedia Manufacturing*, 13, 219–226. doi: 10.1016/j.promfg.2017.09.052.
- Fysikopoulos, A., Pastras, G., Stavridis, J., Stavropoulos, P., Chryssoulouris, G. (2016). On the Performance Evaluation of Remote Laser Welding Process: An Automotive Case Study. *Procedia CIRP*, 41, 969–974. doi: 10.1016/j.procir.2016.01.005.
- Hajjalizadeh, F., Mashhadi, M.M. (2015). Investigation and numerical analysis of impulsive hydroforming of aluminum 6061-T6 tube. *Journal of Manufacturing Processes*, 20, 257–273. doi: 10.1016/j.jmapro.2015.06.027.
- Hong, K.-M., Shin, Y.C. (2017). Prospects of laser welding technology in the automotive industry: A review. *Journal of Materials Processing Technology*, 245, 46–69. doi: 10.1016/j.jmatprotec.2017.02.008.
- https://www.steelnumber.com/en/steel_composition_eu.php?name_id=206. (2024).
- https://www.steelnumber.com/en/steel_composition_eu.php?name_id=218. (2024).
- K Srivastava, A., Sharma, A. (2017). Advances in Joining and Welding Technologies for Automotive and Electronic Applications. *American Journal of Materials Engineering and Technology*, 5(1), 7–13. doi: 10.12691/materials-5-1-2.
- Kimchi, M., Phillips, D.H. (2023). *Resistance spot welding: Fundamentals and applications for the automotive industry* (Second edition). Cham: Springer.
- Manoharan, K.A., Bashir, M.N., Zaifuddin, A.Q. (2020). An Overview of Laser Welding of High Strength Steels for Automotive Application. *International Journal of Technology and Engineering Studies*, 6(1), 23–40. doi: 10.20469/ijtes.6.10004-1.

- Mei, L., Yan, D., Chen, G., Xie, D., Zhang, M., Ge, X. (2015). Comparative study on CO₂ laser overlap welding and resistance spot welding for automotive body in white. *Materials & Design*, 78, 107–117. doi: 10.1016/j.matdes.2015.04.031.
- Mei, L., Yi, J., Yan, D., Liu, J., Chen, G. (2012). Comparative study on CO₂ laser overlap welding and resistance spot welding for galvanized steel. *Materials & Design*, 40, 433–442. doi: 10.1016/j.matdes.2012.04.014.
- Miturska, I., Rudawska, A. (2021). Structural factors influence on strength properties of S235JR steel welded joints. *Journal of Physics: Conference Series*, 1736(1), 012004. doi: 10.1088/1742-6596/1736/1/012004.
- Miturska, I., Rudawska, A., Pawlak, P., Stančėková, D., Chyra, M. (2017). Comparative Analysis of Welded and Adhesive Joints Strength Made of Acid-Resistant Stainless Steel Sheets. *Advances in Science and Technology Research Journal*, 11(4), 97–102. doi: 10.12913/22998624/78165.
- Perka, A.K., John, M., Kuruveri, U.B., Menezes, P.L. (2022). Advanced High-Strength Steels for Automotive Applications: Arc and Laser Welding Process, Properties, and Challenges. *Metals*, 12(6), 1051. doi: 10.3390/met12061051.
- PN-EN 10002-1:2004—*Metallic materials—Tensile testing—Part 1: Method of test at ambient temperature*. (2004).
- Rossini, M., Spena, P.R., Cortese, L., Matteis, P., Firrao, D. (2015). Investigation on dissimilar laser welding of advanced high strength steel sheets for the automotive industry. *Materials Science and Engineering: A*, 628, 288–296. doi: 10.1016/j.msea.2015.01.037.
- Szala, M., Łukasik, D. (2018). Pitting Corrosion of the Resistance Welding Joints of Stainless Steel Ventilation Grille Operated in Swimming Pool Environment. *International Journal of Corrosion*, 2018, 1–7. doi: 10.1155/2018/9408670.
- Uchihara, M. (2011). Joining technologies for automotive steel sheets. *Welding International*, 25(4), 249–259. doi: 10.1080/09507111003655341.
- Xu, T., Shi, Y., Cui, Y., Liang, Z. (2023). Effects of Magnetic Fields in Arc Welding, Laser Welding, and Resistance Spot Welding: A Review. *Advanced Engineering Materials*, 25(5), 2200682. doi: 10.1002/adem.202200682.

SURFACE TOPOGRAPHY CREATION OF MACHINE ELEMENTS AFTER CARBURIZING PROCESS WITH APPLICATION OF BURNISHING METHOD

KSZTAŁTOWANIE TOPOGRAFII POWIERZCHNI ELEMENTÓW MASZYN PO NAWĘGLANIU Z WYKORZYSTANIEM METODY NAGNIATANIA

Lidia GAŁDA^{1,*} 

¹ Department of Machines Technology and Production Engineering, Faculty of Mechanical Engineering and Aeronautics, Rzeszow University of Technology, Powstańców Warszawy 12, 35-959 Rzeszów, Poland

* Corresponding author: lgktmiop@prz.edu.pl

Abstract

Various types of bushings or pins are widely used in the machinery industry, i.e. in the automotive industry, agricultural machinery and production lines. Such machine components operate in a diverse environment, not infrequently in polluted or dusty environments and these components may be subjected to intensive wear. Particles circulating in various types of machine kinematic pairs contribute to accelerated or even emergency wear of the equipment. One way to prevent such dangerous failures is to use an additional machining to create dimples in the surface, which are a place to collect lubricant but also abrasive particles. The article presents a method of burnishing a cylindrical surface after carburizing treatment and after hardening, after which the hardness of the surface layer was about 60 HRC. As a result of using appropriate tools, it was possible to create regular and reproducible dimples in the surface. A surface topography parameter was also proposed, which makes it possible to evaluate the increase in oil capacity of the created cavities quickly and with high quality standards.

Keywords: carburizing, texturing, burnishing, surface topography, analysis of variance

Streszczenie

Różne rodzaje tulei lub sworzni są szeroko stosowane w przemyśle maszynowym, tj. w przemyśle motoryzacyjnym, maszynach rolniczych i liniach produkcyjnych. Takie elementy maszynowe pracują w zróżnicowanym otoczeniu, nierzadko w środowisku zanieczyszczonym czy zapyłonym, a elementy te mogą być narażone na szybkie zużycie. Cząstki krążące w różnego rodzaju kinematycznych węzłach maszyn przyczyniają się do przyspieszonego lub nawet awaryjnego zużycia urządzeń. Jednym ze sposobów zapobiegania takim niebezpiecznym awariom jest stosowanie dodatkowej obróbki w celu ukształtowania wgłębień w powierzchni, które są miejscem gromadzenia substancji smarującej, ale również cząstek ściernych. W artykule przedstawiono sposób nagniatania powierzchni walcowej po obróbce nawęglaniem i po hartowaniu, po których twardość warstwy wierzchniej wynosiła około 60 HRC. W wyniku zastosowania odpowiednich narzędzi udało się ukształtować regularne i powtarzalne wgłębienia w powierzchni. Zaproponowano również parametr topografii powierzchni, który umożliwia szybką i spełniającą wysokie standardy jakościowe, ocenę wzrostu pojemności olejowej kształtowanych wgłębień.

Słowa kluczowe: nawęglanie, teksturowanie, nagniatanie, topografia powierzchni, analiza wariancji

1. Introduction

The bushings and pins are found a variety of sizes and shapes, allowing them to be widely used in industry. These elements are used in many branches, such as automotive, aviation, agricultural machinery,

construction and often specifically in the construction of assembly equipment. The requirements of machine elements that work in the environment of high contamination and under high load is to limit the abrasive wear. One of the methods to prevent the wear is the carburizing process, which is applied to low-



alloy steels in order to modified the properties of the surface layer of the material in further processing phases. After carburizing process the hardening and tempering is used to increase the hardness of the surface layer and the core retains of high ductility. In some applications such treatment is sufficient, but in special cases it may not be enough. For example in sliding pairs of mono-materials of types: steel-steel or steel-cast iron which are susceptible to adhesive wear. Taking into account the mechanism of seizure we may counteract by dimples creation on the sliding surface. One postulate for creation a favorable surface layer to reduce seizure is to form such a micro-geometry that allows for adequate oil capacity and frequent interruption of frictional contact (Nosál, 1998; Nosál, 2002). It is worth to notice that the valleys creation was firstly applied to cylinder liners and it was the honing process. Nowadays, the laser method is usually used for dimple texturing in the zones of cylinder where is a slow motion of piston (Anderson et al., 2007; Dumitru et al., 2003). The wear resistance of textured surfaces is greater than those with the coated surfaces with CrN and DLC of high hardness (Etsion et al., 2006). In most cases the dimples are in spherical shape but they may be in various sophisticated shapes, because the shape is important factor that influence the performance. Results presented by (Galda, 2008; Galda et al., 2010) showed that the dimple in shape of drop oriented deeper side to the movement direction were superior to those of spherical dimple and to untextured surfaces in the tests of seizure resistance of sliding pair consisted of steel and cast iron elements. A degree of surface coverage with dimples is also very important factor and strongly effects on tribological characteristics. At high load and low speed the most favorable outcome were found with the texture coverage of about 10% (Galda et al., 2011). Only on untextured surfaces were observed deep scratches after seizure. Textured surfaces contained some small, it is shallow and short scratches which were stopped by dimples and in some cases seizure did not occur. Research conducted with sliding pair of type steel-steel with one textured element at medium load, low speed and starved lubrication conditions resulted in more than twice reduction in friction coefficient (Galda et al., 2016). On the textured surface no signs of wear were observed, while untextured surface (after grinding) was locally deformed, mainly the peaks were flattened. In these conditions the texture coverage of 3% was superior to other cases. Depth of dimples is another aspect that should be analyzed and selected according to the operating conditions, but there might be a problem with creation dimples on hard materials. The dimples usually are from a few to several tens of micrometers and the machining of the hard-to-

machine materials may be difficult or sometimes impossible with some machining methods. Typically, it is assumed that materials of hardness greater than 45 HRC are in group of the hard-to-machine materials. Hardness of materials after carburizing and hardening is of about 60 HRC, but taking into account the advantages in wear resistance increase is worth to try to create dimples on such surfaces.

This paper presents the results of a study on the burnishing process of 16MnCr5 steel after carburizing and hardening to obtain dimples on sliding surfaces in specific depth and arrangement.

2. Research methodology

In the article the burnishing process of carburized surface layer of 16MnCr5 steel is examined. Steel 16MnCr5 is a structural steel for parts that are surface-hardened and which is most often used in the construction of machinery operating in hard conditions, subjected to wear.

The chemical composition of 16MnCr5 steel is given in Tab. 1.

Table 1. Chemical composition of 16MnCr5 steel (PN-EN ISO 683-3:2022-07)

C (%)	Si (%)	Mn (%)	P (%)
0,14-0,19	≤ 0,40	1,00-1,30	≤ 0,025
S (%)	Cr (%)	Fe (%)	
≤ 0,035	0,8-1,1	rest	

In Table 2 the selected properties of steel 16MnCr5 are presented.

Table 2. Selected properties of steel 16MnCr5 (http, 2024)

Hardness after softening annealing	≤ 207 HB
Hardness after carburizing, hardening and tempering	≥ 60 HRC
Tensile strength R _m , after hardening and tempering at 200°C	820 MPa (16 < d, mm ≤ 40)
Density	7,85 g/cm ³
Temperature of carburizing	880–980°C

Hardness of about 60 HRC after complex treatment of carburizing, hardening and tempering concerns the surface layer and the depth of the layer is usually up to 2 mm.

Samples in shape of shafts in diameter of 30 mm were subjected to carburizing, hardening and tempering and the obtained hardness of surface layer was

approximately of 58 HRC. A precision turning process was used to remove a scale after the heat treatment. Then the burnishing process was used with application a specific burnishing head (Gałda L., Koszela W., 2018). This tool was designed to be easily mounted on universal machines. Figure 1 shows the scheme of the burnishing head. In order to cause the impact of the burnishing element on the surface with high energy, the head uses a cam mechanism and a statically pressed spring. Drive of the cam is carried out by a motor, which is included in the head.

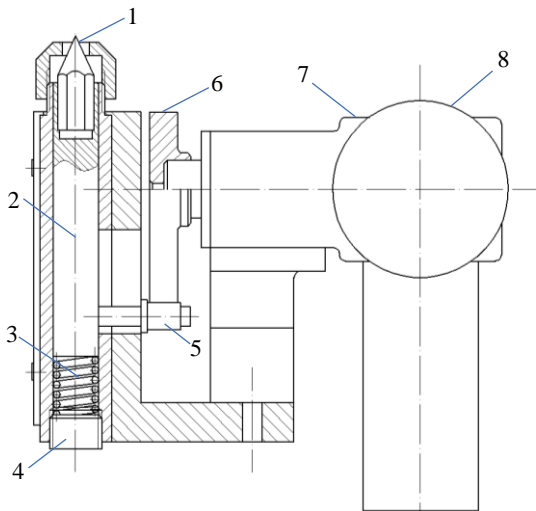


Fig. 1. Scheme of the burnishing head: 1 - burnishing element, 2 – holder, 3 – spring, 4 – adjustment screw, 5 – holder lug, 6 – cam, 7 – gearbox, 8 – motor (Gałda L., Koszela W., 2018)

For the texturing, the tooling used was a cemented carbide G10 burnishing element with a hardness of 1400 HV30. The depth of dimples formed on hard materials depends mainly on the energy of the burnishing element impact. In this case, a hard heavy burnishing element (Fig. 2) and a spring with high stiffness were used, which made it possible to realize texturing effectively.



Fig. 2. Photo of burnishing element from cemented carbide G10

Diameter of dimple is a result also of the burnishing element tip radius. The arrangement of dimples on processing surfaces depends on the technological parameters such as feed, number of cams and rotation speed of cam(s). Thus, there are

several technological parameters that can be controlled in order to achieve the appropriate surface topography after burnishing process.

After complex processing of the shaft made from steel 16MnCr5, its surface was subjected to burnishing process at different technological parameters. The photos of the exemplified burnished surfaces are shown in Fig. 3.

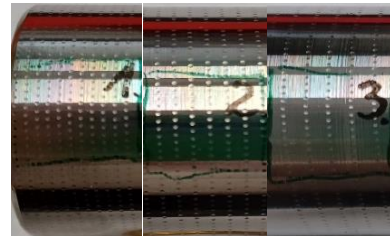


Fig. 3. Photos of shaft surfaces after burnishing with three different feed rate

The technological parameter of burnishing process that was assumed to control was the feed at three levels of variation in the range of 1 - 2 [mm/rev] (Tab. 3).

Table 3. Values of feed during the burnishing process

Surfaces number (fig. 3)	feed f [mm/rev]
1	1
2	1.5
3	2

After burnishing process of carburized surface of steel 16MnCr5 the surface topography was studied with application of an instrument the Form Talysurf i-Series PRO (Taylor Hobson).

To obtain an representative areas of each burnished surfaces, the measured zone was 5 mm x 5 mm. Because the aim of this research was to assess the possibility to form dimples on hard surface after carburizing process, mainly surfaces topography parameters connected with the valleys were analyzed: Svk (reduced valleys depth), Svi (coefficient of keeping the fluid in valleys) and Vvv (void volume per assumed area). The values of selected surface topography parameters were quoted according to standard PN-EN ISO 25178-2:2022. Also some important geometrical parameters of selected dimples were assessed and compared to values of surface topography parameters obtained at different feed rates.

An optical microscope of type Axio Vert.A1 (Zeiss) was used to observe the cross-section of surface layer after carburizing. The image of the cross-section was taken at 12.5x magnification (Fig. 4).



Fig. 4. Image of the cross-section after complex heat treatment with carburizing of steel 16MnCr5 (12.5x magnification)

Depth of the hardened surface layer after complex heat treatment with carburizing process was approximately equal to 600 μm.

3. Results and discussion

Figure 5 shows photos, images and Sk family parameters with shape of Abbott-Firestone curves (bearing area curves) of each burnished surface at varying feeds. Analyzing the surface data, one may noticed that the dimples in circle shape and in regular arrangement are clearly visible on each photos and images, so without any doubts this burnishing method is effective in dimples creation on very hard materials.

The distance between lines of dimples increase with the feed increase and is exactly as the feed value. The number of dimples in lines is on average the same in each case and in further calculation is assumed constant and integer and equal to 6. After removing the form of the measured surface (from shaft) the height is quite comparable, so the depth of dimples should be similar. The reduced depth of valleys is much greater in value than the reduced height of peaks but also from the surfaces core. The shapes of Abbott-Firestone curves are characteristic for the surfaces with valleys presence.

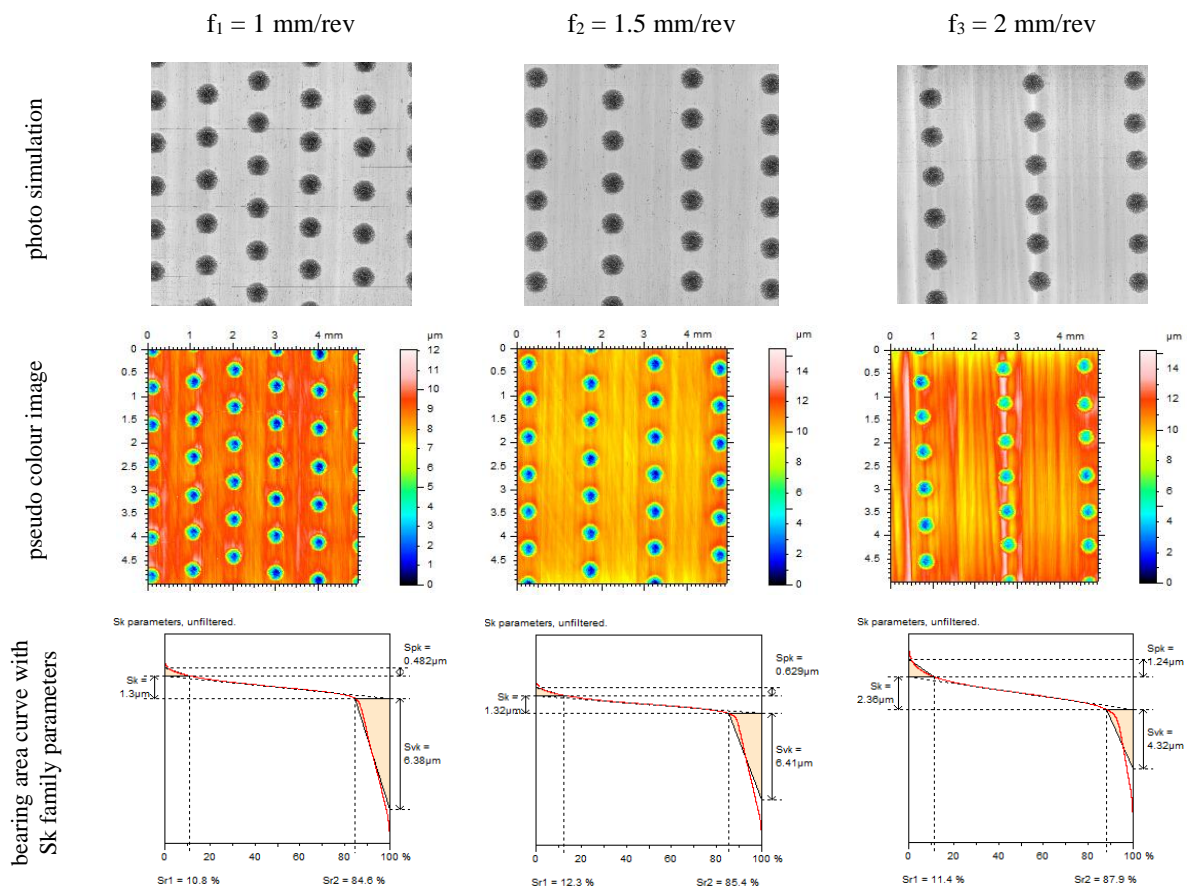
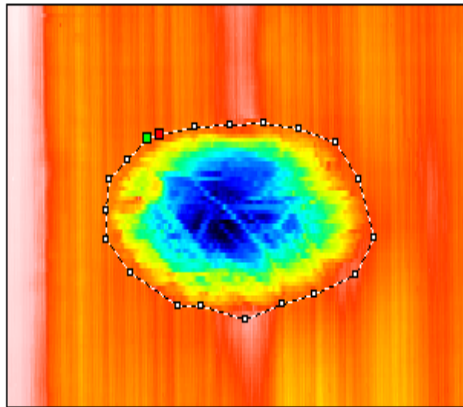


Fig. 5. Selected surface photos, images and bearing area curves after burnishing process with different feeds: $f_1 = 1 \text{ mm/rev}$, $f_2 = 1.5 \text{ mm/rev}$, $f_3 = 2 \text{ mm/rev}$

It would be convenient to assess the oil capacity of created dimples with adequate surface topography

parameters. In order to verify the suitability of the selected surface topography parameters for determining

the changing cavity volume, the dimensions of individual cavities were determined and the volume of created by burnishing process cavities was calculated. A view of single dimple analysis for surface and volume calculation are presented in Fig. 6 and a selected profile for depth and width identification is presented in Fig. 7.



	Hole	Peak
Surface [mm ²]	0.132	0.0122
Volume [μm ³]	516022	2474
Max. depth/height [μm]	9.11	1.16

Fig. 6. View of single dimple created in burnishing process

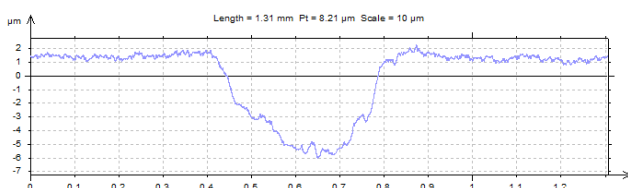


Fig. 7. Profile extracted from a single cavity at its deepest point

Calculations of individual dimple surface and volume were made with Mountains application and it was enough to point the analyzed zone. The dimple depth was assessed with surface profile application (parameter Pt), but to evaluate the dimple width the function measurement in Mountains application was used.

The important geometrical parameters of individual cavities after burnishing process at different feed with statistical analysis are presented in Tab. 4.

There are known solutions for creating textures in hard materials by grinding the surface with specially constructed grinding wheels (Stępień, 2006). The dimples reached 30 μm and their shape on the surface resembled scratches rather than gently rounded circles or ellipses.

A technique for creating dimples in sliding surfaces that has found widespread use in industry is laser surface texturing. Depending on the type of material, it is possible to produce textures of varying

depths but usually no larger than a few tens of micrometers and in almost any shape (Etsion, 2005).

Table 4. Values of geometrical parameters of single dimples after burnishing process of carburized steel 16MnCr5

feed f [mm/rev]	geometrical parameters of cavities			
	depth [μm]	width [μm]	surface [mm ²]	volume [μm ³]
1	8.74	431	0.127	454 169
	9.70	432	0.137	520 144
	9.23	432	0.131	496 510
average	9.22	431.7	0.132	490 274
standard deviation	0.48	0.58	0.005	33 427
1.5	10.10	438	0.143	569 823
	10.10	440	0.141	576 379
	9.88	431	0.143	546 013
average	10.03	436.3	0.142	564 072
standard deviation	0.13	4.73	0.001	15 979
2	9.24	427	0.132	516 022
	9.07	436	0.131	514 546
	10.20	435	0.130	509 163
average	9.50	432.7	0.131	513 244
standard deviation	0.61	4.93	0.001	3610
difference of average values %	8.7	1.1	8.7	15.1

An effective method, but less commonly used than laser texturing, is abrasive blasting. Using blasting, dimples of up to several tens of micrometers and in any shape depending on the cover used can be achieved (Wakuda, 2003). To texture the carburized surface the prototype burnishing tool was used and it was important to assess also the results repeatability. As one may see primary survey data, the standard deviation values are quite small and the difference of average values is 8.7% (for dimple depth) and only 1.1% (for dimple width). It seems to be the acceptable level. The differences between the transformed values are larger (8.7% for dimple surface and 15.1% for dimple volume), but still in these cases it is acceptable.

It is also useful to illustrate on the graph the changes of selected values with the feed changes in the assumed range (Fig. 8).

As analyzing the raw data of depth and width of single dimple, the stable average values and small standard deviations are observed taking into account results at given feed and with increase feed values. Similar observations were taken in case of transformed data, it is of dimple surface but a little greater spread of volume values was noticed. It seems to be acceptable level of repeatability of dimple dimensions

after texturing the carburizing surface with burnishing application.

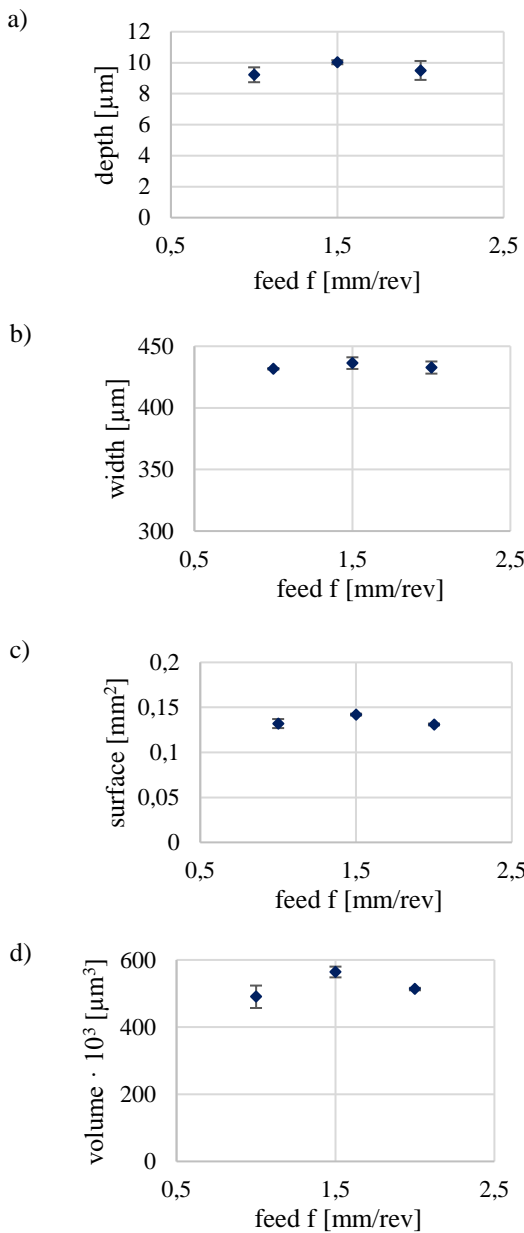


Fig. 8. Average values of depth (a), width (b), surface (c) and volume (d) of single dimple with increasing the feed during burnishing process

To verify this statement another method of data analysis was adopted and it was the one-factor analysis of variance. The input factor was the feed in the range of 1 – 2 mm/rev at three levels. The output factors were the geometrical parameters of single dimple created in burnishing process. A significance level of $\alpha = 0.05$ was assumed. Some more details about this statistical method and also the example of implementation are presented in (Gałda et al., 2022). In Tab. 5 the results of the one-way analysis of variance for four selected geometrical parameters of single dimple are presented.

Table 5. One factor (feed) variance analysis for single dimple geometry parameters

output parameter	F	F_{cr}	p-value
depth	2.42	5.14	0.169
width	1.15		0.376
surface	13.15		0.006
volume	9.27		0.014

Compering the results of calculation one may see that the empirical values F obtained for the dimple depth and width are smaller than the critical value F_{cr} and also p-values are greater than 0.05. It means that the technological parameter (feed) has no significant effect on these geometrical parameters of single dimples. Statistical one-way analysis showed the significant effect of feed on the surface and volume of single dimple, because empirical values F exceed the critical value F_{cr} and p-values were smaller than 0.05, but one should be cautious with the assessment of the influence on transformed parameters. Especially in this case when the exceed is rather small and the process was realized with prototype tool.

The results of the measurements of selected surface topography parameters are shown in Tab. 6.

Table 6. Values of selected parameters of surface topography after burnishing process of carburized steel 16MnCr5

feed f [mm/rev]	surface topography parameters			
	Sa [μm]	Svk [μm]	Svi [-]	Vvv $\cdot 10^3$ [mm^3/mm^2]
1	1.05	4.67	0.305	0.528
1.5	1.02	3.49	0.281	0.505
2	1.00	3.03	0.205	0.328
difference %	5.00	54.13	48.78	60.98

It was assumed that the dimples depth should be similar, so with the decreasing the number of dimples the average amplitude parameters should also decrease, but probably not too much. Taking into account the most popular amplitude parameter Sa that defined an average arithmetical deviation of surface irregularities, the decrease in Sa value is of 5% comparing surfaces of the biggest and smallest number of dimples. From functional parameters the Svk and Svi were selected and the decrease in reduced depth of valleys Svk was of over 54% while the coefficient of storing the fluid in valleys Svi decreased of almost 49% with the increase of feed in burnishing the surface. Another functional parameter of surface topography that may be more adequate for comparing the fluid accommodation in surface valleys that was

analyzed it was V_{vv} . This parameter is defined by valley volume per square millimeter. As the feed rate increased, the volume V_{vv} decreased by almost 61%, caused by the reduced number of cavities. Summarizing, the analysis of surface topography parameters, one may conclude that the average height parameter was changed insignificantly (5%) and selected functional parameters connected with the dimple depth or volume decreased significantly of about 49-61%. It also means that with changing the feed one may control the oil capacity of dimples created in burnishing process.

To compare values of surface topography parameters connected with dimples, the volume of single cavities should be multiply by numbers of created cavities in burnishing process. In this analysis values from the 5 mm x 5 mm area were compared and the results are presented in Tab. 7.

Table 7. Number of dimples after burnishing process in the assumed zones and total volume of cavities

feed f [mm/rev]	parameters of cavities	
	number of dimples, n	total volume, $V \cdot 10^3$ [μm^3]
1	30	14 708
1.5	24	13 538
2	18	9 239
difference %	66.67	59.20

Decreasing the feed during burnishing the number of dimples increased significantly, in the analyzed case it was of over 66%, what resulted in the total volume increase of textured dimples of almost 60% in the analysed zone. Comparing this increase with these obtained with the surface topography parameters application, the highest similarity is obtained with the parameter V_{vv} , which is equal to 60.98%. Parameter V_{vv} expresses the oil capacity in mm^3 per mm^2 of surface area and probably that is the reason that correlates strongly with calculated separately dimples volumes. Summarizing, the parameter V_{vv} can be used to quickly assess the increase in oil capacity with high measurement accuracy after burnishing process with different technological parameters processing.

4. Conclusions

The burnishing process may be used to effectively form the dimples in the surface of a hard surface layer after carburizing. Obtained texture was with acceptable repeatability and in expected shape. The arrangement of the dimples depends on the technological parameters. With smaller feed, the number of dimples is greater, what effects on the oil capacity increase.

Instead of calculation individual dimples geometrical parameters, which is time consuming, the surface topography parameter V_{vv} may be used to assess the increase in oil capacity caused by texture creation with satisfactory accuracy.

References

- Andersson P., Koskinen J., Varjus S., Gerbig Y., Haefke H., Georgiu S., Zhmud B., Buss W. (2007). Microlubrication effect by laser-textured steel surfaces. *Wear* 262, 369-379.
- Dumitru G., Romano V., Weber H. P., Haefke H., Gerbig Y., Pfuge E. (2000). Laser microstructuring of steel surfaces for tribological applications. *Applied Physics A* 70, 485-487.
- Etsion I., Halperin G., Becker E. (2006). The effect of various surface treatments on piston pin scuffing resistance. *Wear* 261, 785-791.
- Gałda L. (2008). Influence of burnished lubricating micro-pockets on tribological properties of sliding elements. Doctoral thesis, Rzeszów.
- Gałda L., Sęp J., Prucnal S. (2016). The effect of dimples geometry in the sliding surface on the tribological properties under starved lubrication conditions. *Tribology International* 99, 77-84.
- Gałda L., Dzierwa A., Pawlus P., Reizer R. (2011). Improvement of tribological properties of co-acting elements by oil pockets creation on sliding surfaces. *Meccanica* 46, 523-534.
- Gałda L., Dzierwa A., Sęp J., Pawlus P. (2010). The effect of oil pockets shape and distribution on seizure resistance in lubricated sliding. *Tribology Letters* 37, 301-311.
- Nosal S. (1998). Tribological aspects of seizure of sliding pairs. Dissertations no. 328, Poznan University of Technology Publishing House, Poznań.
- Nosal S. (2002). Influence of the degree of mutual overlap on adhesive seizure. *Tribologia* 4, 1261-1266.
- Gałda L., Koszela W. (2018). Tool head for the fabrication of a sliding pair, especially a mono-material one. Patent PL no. 230836.
- PN-EN ISO 683-3:2022-07. Heat-treatable steels, alloy steels and free-cutting steels – Part 3: Case-hardening steels. <https://akrostal.pl/stale/16hg-1-7131-16mncr5/> (access on 28.06.2024)
- PN-EN ISO 25178-2:2022. Geometrical product specifications (GPS) – Surface texture: Areal – Part 2: Terms, definitions and surface texture parameters.
- Stepień P. (2006). Fundamentals of creating regular geometric structure of surface in grinding processes. Koszalin University of Technology Publishing House, Koszalin.
- Etsion I. (2005). State of the art in laser surface texturing. *ASME Journal of Tribology* 127, 248-253.
- Wakuda M., Yamauchi Y., Kanzaki S., Yasuda Y. (2003). Effect of surface texturing on friction reduction between ceramic and steel materials under lubricated sliding contact. *Wear* 254, 356-363.
- Gałda L., Pająk D. (2022). Analysis of the application of SiC ceramics as a tool material in the slide burnishing process. *Technologia i Automatyka Montażu*, vol. 1, 45-57. DOI: 10.7862/tiam.2022.1.5.

VOICE CONTROL SYSTEM FOR COLLABORATIVE ROBOT USED IN ASSEMBLY PROCESS

SYSTEM STEROWANIA GŁOSEM DLA ROBOTA KOLABORACYJNEGO WYKORZYSTYWANEGO DO PROCESU MONTAŻU

Jan CZYŻEWSKI^{1,*} 

¹ Rzeszów University of Technology, Aleja Powstańców Warszawy 12, 35-959 Rzeszów, Poland

* Corresponding author: j.czyzewski@prz.edu.pl

Abstract

This work is devoted to the issue of recognizing voice commands by the voice control system of a collaborative robot in an industrial environment. Such a robot will be designed to cooperate with a human during the assembly process. This method of communication significantly facilitates and speeds up work, increasing the efficiency of the assembly process and reducing the operator's workload. However, production halls and other places where assembly takes place are environments filled with sounds with a wide spectrum of intensity and frequency. Such an environment significantly impedes the functioning of the voice control system. This work examined the impact of sound pollution on the robot's command recognition.

Keywords: voice control, collaborative robot, command recognition

Streszczenie

Niniejsza praca poświęcona jest zagadnieniu rozpoznawania komend głosowych przez system głosowego sterowania robotem kolaboracyjnym w środowisku przemysłowym. Robot taki, przeznaczony do współpracy z człowiekiem przy procesie montażu, będzie sterowany za pomocą głosu. Ten sposób komunikacji w znacznym stopniu ułatwia i przyspiesza pracę, pozwalając na zwiększenie wydajności procesu montażu i zmniejszenie obciążenia operatora. Hale produkcyjne i inne miejsca, w których odbywa się montaż są jednak środowiskiem wypełnionym dźwiękami o szerokim spektrum natężenia i częstotliwości. Środowisko takie utrudnia w znacznym stopniu funkcjonowanie systemu sterowania głosem. W pracy tej zbadano wpływ zanieczyszczenia otoczenia dźwiękiem na rozpoznawanie komend przez robota.

Słowa kluczowe: sterowanie głosem, robot kolaboracyjny, rozpoznawanie komend

1. Introduction

Basically, since the creation of the industry, there has been constant effort to improve the production process and its very important part, i.e. the assembly process. One of the trends is the automation and robotization of these processes. Entrusting the assembly process to machines allows to relieve the employee, especially when performing burdensome or monotonous activities. On the other hand, it also ensures high repeatability of the product quality. Naturally, this allows to increase the efficiency of the process, reduce the workload on the employee and

improve his working conditions. Nowadays, robots play an increasingly important role in production plants, which is related to the improvement of their design and the growing range of applications. It also turns out that the availability of specialized assembly specialists on the labor market can be problematic, which is why efforts are being made to support already employed, qualified and experienced employees with robots. This way, one person, with less physical burden, can supervise the work of many robots. Human presence is usually indispensable, and this approach produces beneficial results. However, for



proper cooperation between humans and robots, it is necessary to provide them with appropriate tools for mutual communication. A very convenient system is voice communication, where the operator issues verbal commands that are recognized and executed by the system controlling the operation of robots or other devices. Such systems have a number of advantages. First of all, they use speech, which is a natural human communication tool. Secondly, they allow to bypass switches, switchboards and classic interfaces used on machines. The interfaces themselves are often complicated, have multi-level menus and require long training and getting used to them by the operator. They often differ significantly depending on the model of a specific machine, its manufacturer, etc. It is not always possible to operate them remotely. Voice control can solve these problems. A properly designed voice control system can allow the operator to conveniently find and select the necessary option and issue a command to perform specific activities. This significantly reduces the operator's workload and simplifies his training. Additionally, it can be done remotely. One of the basic challenges when creating such a system is to ensure its effectiveness in the conditions of a production plant. On the one hand, in such a place we are dealing with many sound sources, with a very wide spectrum of intensity and frequency. On the other hand, command recognition must work efficiently and error-free. Both the failure of the system to respond to the issued command and the incorrect interpretation of the issued command may lead to a dangerous situation, threatening both the operator and the machines and manufactured products. Therefore, it is extremely important to thoroughly check the voice recognition system for sensitivity to factors disturbing its operation. This work is devoted to this issue.

Many research works are devoted to the issue of voice control. Nzuva (2021) writes generally about creating an easy way of communication between humans and the machines they operate. Norda et al. (2024) evaluate the usefulness of voice control in industry and its impact on improving work efficiency. Longo et al. (2020) also write about the need to modernize methods of collaboration between humans and devices in the environment of a modern factory. Janiček et al. (2021a), Chmielowiec et al. (2024) and Bingol et al. (2020) work on the problem of controlling robots using voice in industrial applications. Anggraen et al. (2018), Priyadarshana et al. (2022) and Rendyansyah et al. (2022) also focus on controlling robots using voice. Andrew et al. (2021) additionally focus on reducing the costs of such a system. Lavrynenko (2024) deals with the problem of ensuring the proper functioning of a speech recognition system

in a noisy environment. Similarly, Janiček et al. (2021b) examine the problem of the influence of sound intensity on the operation of the system. Voice is considered a good form of communication with universal robots designed to support humans in everyday duties. What is important here is the simplicity of this form of communication, which does not require additional qualifications. Li et al. (2023) and Linda et al. (2020) writes about it. Khan et al. (2021) write about the application of a voice control system in a robotic car. Also, great potential for voice control has been noticed in the case of robots and other devices intended for disabled people. Prostheses replacing limbs can also be voice-controlled - this is described by Oyelami et al. (2023). Piyaneeerant et al. (2022) propose the use of voice control in a robot supporting older people, and Bakouri et al. (2022) in a robotic wheelchair.

2. Materials and methods

A simple scheme for issuing commands to the robot was adopted. The commands are supposed to control the robot's movements (fig. 1). For testing purposes, it was assumed that simple movements along the coordinate system axes were performed by given values, expressed in millimeters. For now, more complex movements, changes in movement speed, or movement values after the decimal point were omitted.



Fig. 1. Hanwha collaborative robot, planned for system testing

Commands consist of single words, representing letters and numbers. These words were taken from the ICAO (International Civil Aviation Organization) phonetic alphabet, also known as the NATO phonetic alphabet (tab. 1 and 2). The main advantage of this coding is its simplicity, unambiguity and resistance to interference. Since the arrangement of syllables that make up individual words of the code is not repeated, even a fragmentary transmission can be understood. Therefore, it is widely used in radio communication,

especially in aviation, where unambiguity and ease of understanding of messages are of key importance. A complete command contains the coordinate in which the robot is to move (X, Y or Z), a + or – sign specifying the direction, and a sequence of numbers specifying the displacement value in mm.

Table 1. Letters in ICAO code

Letter	Code	Pronunciation
A	Alfa	[ˈalfa] <i>alfa</i>
B	Bravo	[ˈbravo] <i>brawo</i>
C	Charlie	[ˈtʃali] <i>czarli</i>
D	Delta	[ˈdelta] <i>delta</i>
E	Echo	[ˈɛko] <i>eko</i>
F	Foxtrot	[ˈfɔks.trot] <i>fokstrot</i>
G	Golf	[ˈgɒlf] <i>golf</i>
H	Hotel	[hoˈtɛl] <i>hotel</i>
I	India	[ˈɪndia] <i>indija</i>
J	Juliett	[ˈdʒuliˈɛt] <i>dżulijet</i>
K	Kilo	[ˈkilo] <i>kilo</i>
L	Lima	[ˈlima] <i>lima</i>
M	Mike	[ˈmaɪk] <i>majk</i>
N	November	[noˈvɛmba] <i>nowember</i>
O	Oscar	[ˈɔska] <i>oskar</i>
P	Papa	[paˈpa] <i>papa</i>
Q	Quebec	[keˈbɛk] <i>kebek</i>
R	Romeo	[ˈromio] <i>romijo</i>
S	Sierra	[siˈɛra] <i>sijera</i>
T	Tango	[ˈtango] <i>tango</i>
U	Uniform	[ˈjuːnɪfɔːm] <i>juniform</i> lub [ˈunɪfɔːm] <i>uniform</i>
V	Victor	[ˈvɪktɔːr] <i>wiktor</i>
W	Whiskey	[ˈwɪski] <i>łyski</i>
X	Xray	[ˈɛks.reɪ] <i>eksrej</i>
Y	Yankee	[ˈjɑːŋki] <i>jancki</i>
Z	Zulu	[ˈzulu] <i>zulu</i>

Table 2. Numbers in ICAO code

Number	Code	Pronunciation
0	Zero	[ˈziro] <i>ziro</i>
1	One	[ˈwan] <i>jan</i>
2	Two	[ˈtu] <i>tu</i>
3	Three	[ˈtri] <i>tri</i>
4	Four	[ˈfoa] <i>fower</i>
5	Five	[ˈfaɪf] <i>fajf</i>
6	Six	[ˈsɪks] <i>siks</i>
7	Seven	[ˈsɛvən] <i>seven</i>
8	Eight	[ˈeɪt] <i>ejt</i>
9	Niner	[ˈnaɪnɪr] <i>Niner</i>

Sound analysis was created in Python using the open source librosa library. Librosa is used for music and sound analysis, helping software developers create applications for working with audio and music file formats using Python. This library can handle both basic and advanced tasks related to sound and music processing.

After separating the speech signal from the surrounding silence, its parameterization is necessary, because it is characterized by a large amount of information redundancy. For this purpose, the method of cepstral coefficients in the mel frequency scale (mel-Frequency Cepstral Coefficients) can be used. As Furui (2009) writes, MFCC is the longest-developed method of human speech parameterization. The signal spectrum obtained by the fast Fourier transform is filtered by a bank of filters covering the entire frequency band of the signal. Mel-cepstral parameters are created from the cepstrum of the signal presented in the mel scale (melcepstrum). The set of filters imitates the characteristics of the human hearing system. The mel scale is obtained by filtering the signal with a bank of filters with a triangular characteristic. The k-th mel-cepstral coefficient corresponds to the content of the k-th band.

The mel-cepstral parameter vector is a vector of cepstrum coefficients in the appropriate mel bands. They are intended to reflect the natural response of the auditory system to stimulation by speech sounds. The mel-cepstral parameters are characterized by low sensitivity to noise.

At the beginning of the algorithm, the speech signal is subjected to a pre-emphasis process, i.e. formative filtering, aimed at weakening low-frequency components and amplifying high-frequency components.

$$x'_n = x_n - ax_{n-1}, \quad (1)$$

where x_n and x'_n are the signal before and after pre-emphasis, respectively, and a is the coefficient (the most commonly assumed value is 0.97).

The next stage is signal framing, i.e. dividing the signal into short fragments called frames. It is possible to use overlap of subsequent time frames. Then windowing is performed using a Hamming window.

$$\text{Ham}(N) = 0,54 - 0,46 \cos\left(2\pi \frac{n-1}{N-1}\right) \quad (2)$$

where N is the frame length, and $n = 1, 2, \dots, N$. Each frame is subjected to the FFT to obtain the power spectrum $|FFT|^2$ or the amplitude spectrum $|FFT|$ depending on the algorithm implementation. The obtained spectrum is subjected to the action of a set of filters. The number of filters and their shape differs depending on the algorithm implementation, but the most common in the literature are triangular filters, whose centers are evenly distributed in a given frequency range on the mel scale. An example set of filters is shown in the figure. At the output of each filter, the band energy is obtained according to the formula:

$$S_m = \sum_{k=1}^N |X_r(k)|^2 H_m(k) \quad (3)$$

where m is the filter number, and X_r is the frame spectrum.

In further calculations, the logarithm of energy is used, which allows to reduce the sensitivity of filters to very loud and very quiet sounds and to model the nonlinear amplitude sensitivity of the human ear. Moreover, the use of the logarithm significantly affects the quality of recognition. The last stage of the algorithm is to apply the discrete cosine transform (DCT). The final values of the MFCC coefficients are calculated as:

$$c_i = \sqrt{\frac{2}{M}} \sum_{m=1}^M \log(S_m) \cos\left(\frac{\pi i}{M}(m - 0,5)\right) \quad (4)$$

where i is the coefficient number and M is the number of filters used. In most recognition systems, i takes values from 1, and the coefficient c_0 is omitted. Often, the logarithm of the frame energy is added to the obtained coefficients:

$$E = \log\left(\sum_{k=1}^N x_k^2\right) \quad (5)$$

It is beneficial for the machine learning process to prepare a sufficiently large number of samples. 100 sound samples were recorded for each letter and digit.

The samples are then subjected to a normalization process.

Audio normalization is the process of applying a constant amount of sound gain to an audio recording. So it is the process of changing the amplitude value of a signal in a consistent way (for all values). Gain would then be the amount by which the sound is changed. This can be a positive or negative value. There are two types of normalization, these are: peak normalization and average normalization.

Average normalization determines the average level of an audio file and similarly raises or lowers it to a target level.

In this case, the peak normalization process is used. This process finds the highest PCM (pulse-code modulation) value or pulse-code modulation value of an audio file. Basically, the audio signal is normalized so that it is related to the loudest point recorded in the audio waveform. The calculation involves subtracting the individual values from the measured peak value. Audio normalization solves the problem of varying loudness levels in a sequence of recordings (fig. 2).

Then, in each of the recorded samples, the silence area was identified and cut out. Silence was defined as sound of intensity not exceeding 30 dB and higher volume pulses whose duration does not exceed 0.5 s (fig. 3).

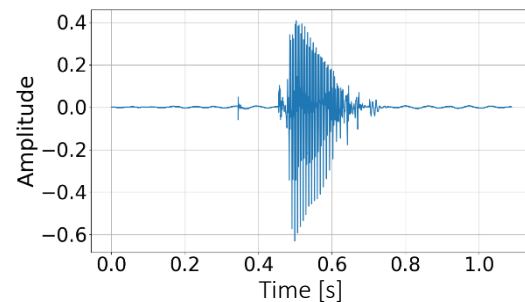


Fig. 2. Single word recording

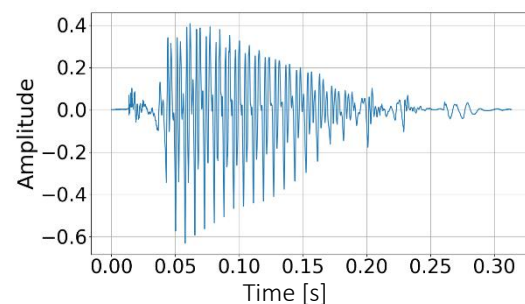


Fig. 3. Single word recording after cutting out the silence

The samples were then subjected to a process called resampling, or changing the sampling rate. The sampling rate is a measure of the number of samples recorded per second from an audio signal. It is measured in hertz (Hz) and indicates how often

a sample of the audio signal is recorded per second. A single sample is a measure of the volume of the audio signal at a specific moment in time. The original frequency of 44,100 Hz is reduced to 16,000 Hz at this stage.

A series of typical MFCC statistics were then determined.

Two types of classifier were used:

- K-NN – k nearest neighbors classifier. Nearest neighbor analysis is a method of classifying observations based on their similarity to other observations. The method was developed in machine learning as a way to recognize patterns in data without having to ensure exact correspondence to any memorized patterns or observations. Similar observations are close together, and dissimilar ones are far away. Therefore, the distance between two observations is a measure of their dissimilarity. Observations that are close together are called "neighbors." When a new observation is presented, the distance from each observation to the model is calculated. The classification of the most similar nearest neighbor observations is determined, and the new observation is placed in the category that contains the largest number of nearest neighbor observations.
- SVM (Support Vector Machines). The SVM algorithm works by mapping data into a multidimensional feature space in a way that allows data points to be categorized, even if the data cannot otherwise be linearly separated. First, a separator between categories is found. Then, the data is transformed in a way that allows the separator to be drawn as a hyper-plane. Once this is done, the characteristics of the new data can be used to predict the group to which a new record should belong.

Sample recordings are shown in the figures (fig. 4 and 5). The recording in conditions of high ambient noise emission is visible in Figure 6.

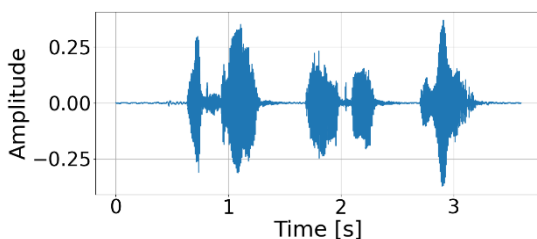


Fig. 4. Example recording of actions in 3 words

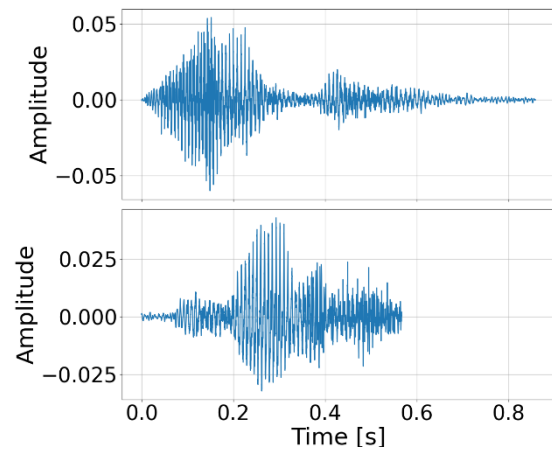


Fig. 5. Division into single commands

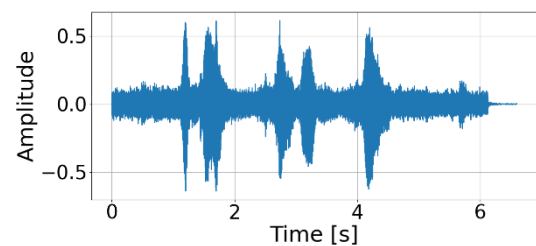


Fig. 6. Example recording of 3-word actions in a noisy environment

The following sets of classifiers and statistics were used in the study:

- 1) nearest neighbor classifier for 5 neighbors, MFCC statistics vector as the basis for classification (KN - S),
- 2) nearest neighbor classifier for 5 neighbors, linear interpolation vector for MFCC (KN - I),
- 3) support vector machine classifier, MFCC statistics vector as the basis for classification (SVM - S),
- 4) support vector machine classifier, linear interpolation vector for MFCC (SVM - I).

In all sets, the silence level was defined at the aforementioned level of 30 dB.

Since MFCC values are tensors dependent on the length of the audio signal, it is not possible to use them directly in machine learning systems. It is necessary to first standardize the lengths of the vectors representing the audio signal. Therefore, two approaches were used to address this issue. The first one consisted in determining the statistics vector based on the MFCC tensor, including: mean, standard deviation, median, minimum, maximum, skewness and kurtosis.

The second approach consisted of interpolating the MFCC components and transforming them into vectors of equal length equal to 100 coordinates. This operation aimed to capture the main features of the audio signal and reduce them to a tensor with

a dimension independent of the signal length. The interpolation method adopted in this case was linear interpolation, which is very fast and does not generate too much additional computational load.

Before determining the MFCC coefficients, each audio signal was normalized by rescaling it to the interval [-1;1]. This made comparing signals of different amplitudes more efficient. This procedure also eliminated the need to normalize the tensors intended for the machine learning model, because the MFCC coefficients were determined on signals of fixed amplitude (fig. 7, 8 and 9).

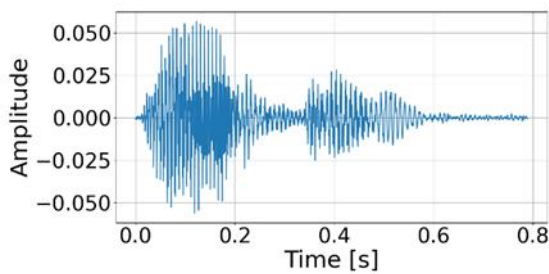


Fig. 7. Example Alpha command

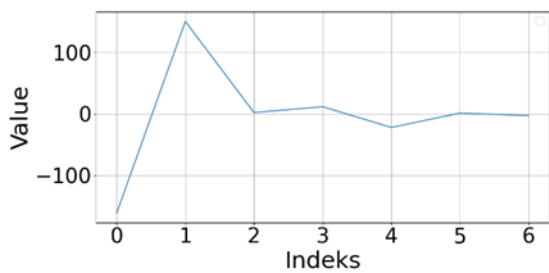


Fig. 8. Statistics graph for the first MFCC coefficient for the Alpha command

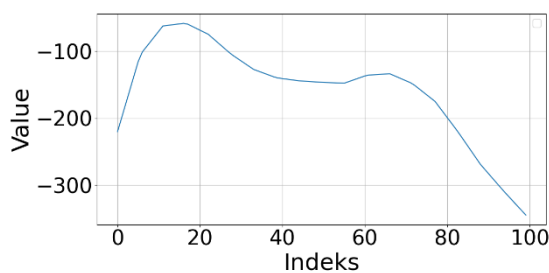


Fig. 9. Interpolation graph for the first MFCC coefficient for Alpha command

3. Results

The process of preparing vectors for machine learning consisted of using 40 previously created samples for each letter and digit. The machine learning process used 80% of the samples for model training and 20% for verification.

The level of accuracy of the models was as follows:

- KN - S: 0.98
- KN - I: 1.00
- SVM - S.: 0.99
- SVM - I: 1.00

Next, the recognition of requests composed of a single command was tested. The results were as follows:

- KN - S: 0.79
- KN - I: 0.92
- SVM - S: 0.85
- SVM - I: 0.95

Then, tests were performed on requests consisting of two commands, which were generated as the Cartesian product of the sets {'a', 'b', 'c'} x {'0', '1', ..., '9'}. The results of the recognition efficiency are as follows:

- KN - S:
 - for single command request: 0.70
 - for two command request: 0.50
- KN - I:
 - for single command request: 0.80
 - for two command request: 0.63
- SVM - S:
 - for single command request: 0.82
 - for two command request: 0.67
- SVM - I:
 - for single command request: 0.88
 - for two command request: 0.80

Table 3. Accuracy results summary

	Accuracy of the model	Accuracy of single command request recognition	Accuracy of two commands request recognition
KN-S	0,98	0,79	0,70
KN-I	1,00	0,92	0,50
SVM-S	0,99	0,85	0,80
SVM-I	1,00	0,95	0,63

4. Conclusions

The results of the conducted studies indicate that the effectiveness of recognizing single voice commands using nearest neighbor classifiers and support vector machine-based classifiers is very high, ranging from 98% to 100%. However, tests performed on requests consisting of one or several commands clearly show that this effectiveness significantly decreases when it becomes necessary to extract a single command from the audio signal. An additional challenge in such cases is the noise present in workshops or production halls. Therefore, the feasibility of using voice control in industrial assembly

automation systems largely depends on the effectiveness of methods for extracting single commands. Consequently, future research should focus on developing methods for precise localization of commands within the analyzed audio signal.

References

- Andrew, A.B., Rajiv, S.A., Jusat, N., Zainuddin, A.A., Subramaniam, K., Rahman, N.A. (2021). Implementation of Low-Cost Voice Command Robot Using Arduino Uno Platform, 2021 IEEE 7th International Conference on Smart Instrumentation, Measurement and Applications (ICSIMA), 2021, pp. 134-139, 23-25 August, 2021, ILMA Journal of Technology & Software Management - IJTSM Vol. 2 Issue. 2. <https://doi.org/10.1109/ICSIMA50015.2021.9526315>.
- Anggraeni, D., Sanjaya, W.S.M., Nurasyidiek, M.Y.S., Munawwaroh, M. (2018). The Implementation of Speech Recognition using Mel-Frequency Cepstrum Coefficients (MFCC) and Support Vector Machine (SVM) method based on Python to Control Robot Arm. IOP Conference Series: Materials Science and Engineering. <https://doi.org/10.1088/1757899X/288/1/012042>.
- Bakouri, M. (2022). Development of Voice Control Algorithm for Robotic Wheelchair Using NIN and LSTM Models, 73(2), 2441-2456. <https://doi.org/10.32604/cmc.2022.025106>.
- Bingol, M. C. & Aydogmus, O. (2020). Performing predefined tasks using the human-robot interaction on speech recognition for an industrial robot. *Eng. Appl. Artif. Intell.*, vol. 95. <https://doi.org/10.1016/j.engappai.2020.103903>.
- Chmielowiec, A., Łysiak K., Vilis J. (2024). Development of a Basic CAM Processor for a Collaborative Robot for Workshop Automation. *Technologia i Automatyizacja Montażu*, 123(1/2024), p. 37-45. <https://doi.org/10.7862/tiam.2024.1.6>.
- Furui, S. (2009). Selected topics from 40 years of research in speech and speaker recognition. Interspeech 2009, Brighton (UK). <https://doi.org/10.21437/Interspeech.2009-1>.
- Janiček, M., Ružarovský R., Velišek, K., Holubek, R. (2021) Analysis of voice control of a collaborative robot. *Journal of Physics: Conference Series* 2021. <https://doi.org/10.1088/1742-6596/1781/1/012025>.
- Janiček, M., Holubek, R., Ružarovský, R., Velišek, K. (2021). Voice frequency impact for voice control of collaborative robots, IOP Conference Series: Materials Science and Engineering, vol. 1009, Oct. 2021. <https://doi.org/10.1088/1757-899X/1009/1/012025>.
- Khan, R.L., Priyanshu, D., Alsulaiman, F.S. (2021). Implementation of Human Voice Controlled Robotic Car. 10th International Conference on System Modeling & Advancement in Research Trends (SMART), 2021, pp. 640-646, 10-11 Dec, 2021, India, <https://doi.org/10.1109/SMART52563.2021.9676319>.
- Ławrynenko O. (2024). Voice Control System for Robotics in a Noisy Environment. *Electronics and Control Systems*, Vol. 3 No. 81. <https://doi.org/10.18372/1990-5548.81.19016>.
- Li, S.-A., Liu, Y.-Y., Chen, Y.-C., Feng, H.-M., Shen, P.-K., Wu, Y.-C. (2023). Voice interaction recognition design in real-life scenario mobile robot applications. *Applied Sciences*, vol. 13, no. 5, pp. 3359. <https://doi.org/10.3390/app13053359>.
- Linda, M., J., Nilesh, V., Rajat, S. (2020). Voice Control Human Assistant Robot. *Proceeding of 2nd VNC; VNC-2020, 2nd National Conference on Technical Advancements for Social Upliftment*, 4th April, 2020 at Vidyavardhini's College of Engineering & Technology (VCET), Vasai, India. <https://doi.org/10.17577/IJERTCONV9IS03084>.
- Longo, F., Padovano, A. (2020). Voice-enabled assistants of the operator 4.0 in the social smart factory: Prospective role and challenges for an advanced human-machine interaction", *Manuf. Lett.*, vol. 26, pp. 12-16, Oct. 2020. <https://doi.org/10.1016/j.mfglet.2020.09.001>.
- Norda, M., Engel, Ch., Rennies, J., Appell, J.-E., Lange, S.C., Hahn, A. (2024). Evaluating the Efficiency of Voice Control as Human Machine Interface in Production. *IEEE Transactions on Automation Science and Engineering* 2024, vol. 21, issue 3. <https://doi.org/10.1109/TASE.2023.3302951>.
- Nzuva, S.M. (2021). Investigating human-machine interfaces' efficiency in industrial machinery and equipment: A Kenyan context", *International Journal of Information Technology, Control and Automation (IJITCA)*, vol. 11, no. 4, pp. 1-8, Oct. 2021. <https://doi.org/10.5121/ijitca.2021.11401>.
- Oyelami A.T., Elegbeji, W.F., Adeniyi, O. (2023). 4-degree-of-freedom voice-controlled robotic arm. *IAES International Journal of Robotics and Automation (IJRA)* 2023, Vol. 12, No. 4, pp. 341-351. <https://doi.org/10.11591/ijra.v12i4.pp341-351>.
- Piyaneeranart, M., Ketcham, M. (2021). Automatically moving robot intended for the elderly with voice control. *International Journal of Online and Biomedical Engineering (iJOE)*, vol. 17, no. 06, pp. 19-48. <https://doi.org/10.3991/ijoe.v17i06.22299>.
- Priyadarshana, V., Yaparathne, Y., Jayasooriya, D., Thennakoon, T., Jayasekara, A., D.P., Chandima, D. (2022). Voice controlled robot manipulator for industrial applications. *Proc. IEEE 13th Annu. Inf. Technol. Electron. Mobile Commun. Conf. (IEMCON)*, pp. 0160-0165, Oct. 2022. <https://doi.org/10.1109/IEMCON56893.2022.9946545>.
- Rendyansyah, R., Prasetyo, A.P.P., Sembiring, S. "Voice command recognition for movement control of a 4-DoF robot arm", *ELKHA*, vol. 14, no. 2, pp. 118, Oct. 2022. <https://doi.org/10.26418/elkha.v14i2.57556>.